https://doi.org/10.5194/essd-2025-335
Preprint. Discussion started: 11 July 2025
© Author(s) 2025. CC BY 4.0 License.

[andreapioferreri@gmail.com] [marilena.filippucci@uniba.it]

The new seismic catalog of the Gargano area (Southern Italy) after a decade of seismic monitoring by OTRIONS network

Andrea Pio Ferreri[1,*], Annalisa Romeo[2], Rossella Giannuzzi[1], Teresa Ninivaggi[3], Marilena Filippucci[1,4,*], Gianpaolo Cecere[3], Luigi Falco[3], Maddalena Michele[4], Giulio Selvaggi[4], and Andrea Tallarico[1,4]

[1]Dipartimento di Scienze della Terra e Geoambientali, Università di Bari - Aldo Moro, Bari, Italy
[2]Istituto Nazionale di Geofisica e Vulcanologia, Osservatorio Vesuviano, Napoli, Italy
[3]Istituto Nazionale di Geofisica e Vulcanologia, Sezione Irpinia, Grottaminarda (AV), Italy
[4]Istituto Nazionale di Geofisica e Vulcanologia, Osservatorio Nazionale Terremoti, Rome, Italy
[*]Correspondence: andreapioferreri@gmail.com, marilena.filippucci@uniba.it

Abstract. The Gargano Promontory (hereafter GP) has attracted the attention of seismologists in recent years for its peculiarities regarding the high rate of low-magnitude seismicity and focal depths in the lower crust. These peculiarities have been highlighted thanks to the new data provided by the OTRIONS seismic network (hereafter OT), installed in 2013 in the GP area, consisting of 15 short-period seismometers, thanks to a fruitful collaboration between UniBa (University of Bari Aldo Moro) and INGV (Istituto Nazionale di Geofisica e Vulcanologia). The first available seismic catalog refers to the first 7 year of the network operation (2013-2018) suffered of some technological problems of the acquisition system. Thanks to improvements in the data transmission system, these problems were overcome in 2019 and now the OT network data are available in real time. In order to include the most recent seismicity and to cover the temporal gaps existing in the previous catalog, we thoroughly reviewed the 24h seismic recordings, collected over the decade after the installation, by employing an automatic detect and picking software (CASP, Complete Automatic Seismic Processor). More than 6900 seismic events were initially identified. Through careful manual review, approximately 60% were confirmed as local earthquakes, and the others were recognized as quarry blasts or false/poorly-located events. Manual revision significantly improved the quality of P- and S-phase picks, which led to more accurate earthquakes locations by both linearized and non-linear algorithms obtaining 2 catalogs both here released. This study highlights the value of semi-automated analysis for seismic catalog compilation but manual revision is still necessary. The quality of the catalogs was assessed in detail using statistical parameters and a new formula for the location quality. The completeness magnitude of the new catalogs is as low as 0.82. The noise affecting the network was also evaluated. This study confirms the importance of the OT local network for seismic hazard analysis and provides a useful data set for seismotectonic and geophysical studies in a long under-monitored region.

https://doi.org/10.5194/essd-2025-335
Preprint. Discussion started: 11 July 2025
© Author(s) 2025. CC BY 4.0 License.

Open Access Earth System Science Data Discussions

1 Introduction

Monitoring small to moderate magnitude earthquakes is essential to understand the seismotectonic, seismic hazard and strong-motion characteristics in region unexplored and to this end, the installation of dense seismic networks is essential. It is observed that the increasingly dense coverage provide better data quality that, together with novel technologies in observational seismology, have significantly improved the earthquake detection capabilities worldwide (refer to Li (2021) for a review).

Of particular interest for Southern Italy are the examples of installation of permanent or temporary local seismic networks to improve the detection threshold of the Italian National Seismic Network (RSN) managed by INGV. In the followings, some example of local seismic monitoring in southern Italy are reported. The Irpina Seismic Network (ISNet) was deployed in 2005 and provided valuable information on the seismicity of the Southern Apennines region, contributing to the understanding of seismogenic processes in an area hit by the strong earthquake of 1980, November 23, $Ms = 6.9$ earthquake, in a period in which the coverage of RSN was very poor (Iannaccone et al., 2010). On the island of Ischia (Southern Italy), the results of the local seismic network contribute to research on volcanic and seismic risk assessment, providing data that can inform disaster preparedness and response strategies and has been significantly improved after the earthquake of 21 August 2017 ($M_d = 4.0$), that caused two fatalities, (Tramelli et al., 2024) and it was fundamental to record and constraint the few and small ($M_{max} = 2.5$) aftershocks. In the Val d'Agri (Southern Italy) the local seismic network INSIEME, composed of seismic stations equipped with broadband posthole sensors positioned in wells with depths from 6 m to 50 m, is functional to monitor the microseismicity induced both by hydrocarbon extraction and by activities related to the water supply of the region (Stabile et al., 2020). In the Pollino region, several seismic networks have been operational, following a 4-year increase in seismicity occurred in 2010. During this period, a group of temporary seismic stations from the INGV (Govoni et al., 2023) and the Deutsches Geo Forschungs Zentrum (GFZ) (Passarelli et al., 2012, 2017) (Passarelli et al., 2012) were installed in order to improve the real-time earthquake identification capability of the Italian National Seismic Network. De Gori et al. (2022) describe how the Pollino seismic networks were essential to detect and analyze the seismicity and contributed to the study of the deformation dynamics highlighting the presence of an active and complex fault system.

From the examples above, without claiming to be exhaustive with respect to the wide diffusion of local networks in Italy and worldwide, it can be argued that the multiplication of seismic stations involves, as a consequence of the large amount of seismic data, a strong effort in terms of human and information technology resources and therefore also raises the question of a non-trivial increase in costs and it is precisely the trade-off between scientific benefits and costs that, according to Ebel (2008), would requires a broader public debate even though it is indubitable the improvement in the seismological knowledge for hazard mitigation and public safety issues. Therefore, earthquake monitoring is the basis of observational seismology and earthquake catalogues are its main product, essential in all the seismological based studies. The amount of continuous data available 24h moves the seismological community toward automated processing approach to the arrival time picking of P and S waves and to earthquake location.

In this paper our focus is on the GP area that belongs to the Apulia region (Southern Italy) which is part of the Adria plate, shown in Fig. 1a (refer to Del Gaudio et al. (2007); Pierri et al. (2024) for a review). GP represents the northernmost sector of

https://doi.org/10.5194/essd-2025-335
Preprint. Discussion started: 11 July 2025
© Author(s) 2025. CC BY 4.0 License.

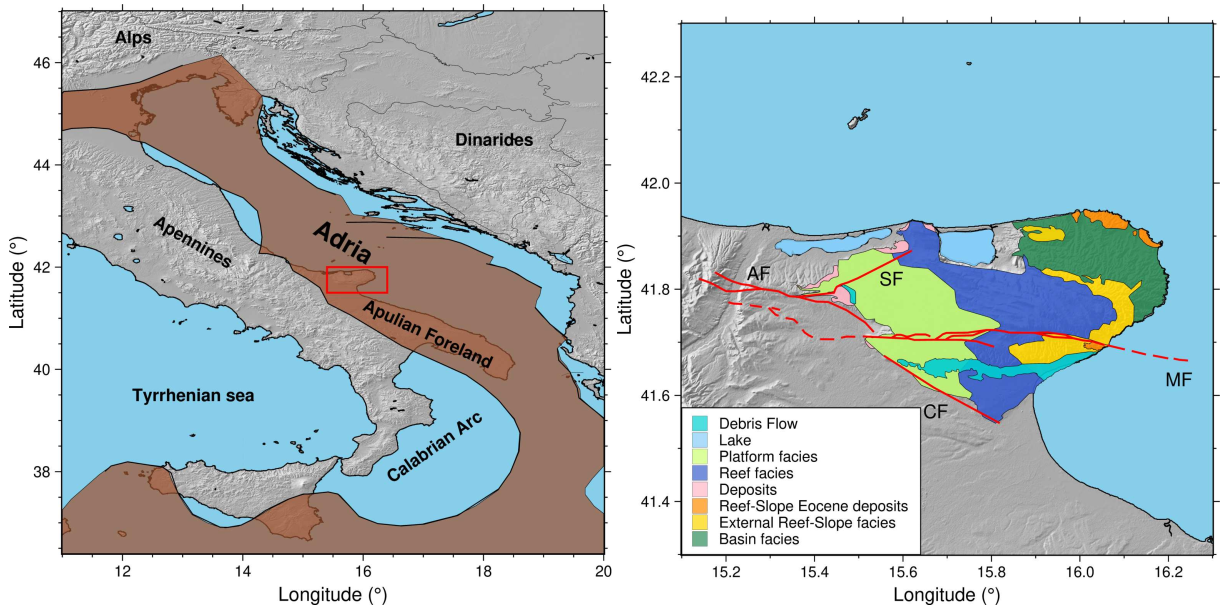

(a) (b)

Figure 1. a) Brown area represents the Adria microplate with the studied area of the GP in the red square. b) Generalized geological map of the GP area highlighting the principal stratigraphic sequences and fault systems.

the Apulian foreland and is predominantly composed by slightly deformed carbonatic successions (Del Gaudio et al., 2007). A generalized geological map, in which the principal stratigraphic sequences and fault systems of the GP area are represented, is shown in Fig. 1. Several studies have identified some of the major faults, shown in Fig. 1b, like the Mattinata fault (MF) (Chilovi et al., 2000), the Apricena fault (AF) (Patacca and Scandone, 2004), the Candelaro fault (CF) (Mongelli and Ricchetti, 1970), and the Sannicandro fault (SF) (Salvi et al., 1999), although their characteristics and evolution still remain under discussion. In addition, according to Doglioni et al. (1994), the GP is also characterized by a parallel fault system with an east-west orientation, causing uplift in this region. Six strong earthquakes throughout history, with magnitudes greater than 6, struck the GP area, the biggest of which in 1627 with $M_w = 6.7$ (Rovida et al., 2016) while, in the instrumental era, the seismicity of GP is characterized by low magnitude seismicity with high seismic rate. A $M_w = 4.8$ earthquake occurred in March 2025, the maximum magnitude instrumentally recorded in this area (data from https://terremoti.ingv.it/ accessed on 30^{th} May 2025).

In recent years, thanks to the installation of the OT local seismic network (see 2.1 for an exhaustive description) the seismic monitoring of GP was strongly enhanced allowing the recording and detection of a high number of micro-earthquakes. As for the above mentioned examples, new insights in the seismic attenuation (Filippucci et al., 2019a; Lucente et al., 2023) and thermo-rheological properties of the upper and lower crust also related to fluid circulation (Filippucci et al., 2019b; Lavecchia et al., 2022) and on seismogenic structures (Miccolis et al., 2021) that could be responsible of both the shallow and deep seismicity in the GP crust were achieved by using the first seismic catalog collected and released so far (Filippucci et al., 2021). This catalog is subject to some limitations as it was collected in real-time mode, at a time when the OT network was

https://doi.org/10.5194/essd-2025-335
Preprint. Discussion started: 11 July 2025
© Author(s) 2025. CC BY 4.0 License.

suffering from technical problems in data transmission (see 2.1). With the aim of obtaining a more complete catalog of GP seismicity, in this work we adopted the Complete Automatic Seismic Processor (CASP), (Scafidi et al., 2019), to analyze 10 years of seismic recordings, from 2013 to 2022, in non-real time mode. CASP has been proven to be fast in processing big amount of 24h seismograms, to be consistent in arrival times picking of P and S phases allowing accurate event location (Spallarossa et al., 2021). The seismic catalog obtained automatically by CASP was manually revised to evaluate the reliability in detection and location. The manual revision of P and S phase arrivals provided two seismic catalogs, by using both linearized (Hypo71) and non-linear (NonLinLoc) algorithms. The quality of the locations was assessed by using the location parameters in a quality factor formula. Magnitudes were also computed by using Di Bona (2016) attenuation law. An analysis of the performance of the seismic network was assessed.

2 Gargano seismic network (GSN)

The microseismicity in the Gargano Promontory and surroundings is monitored by the OTRIONS Seismic Network (FDSN code OT, University of Bari "Aldo Moro", 2013), managed by UniBa (Tallarico, 2015), and by the Rete Sismica Nazionale (FDSN code IV, Istituto Nazionale di Geofisica e Vulcanologia (INGV), 2005) managed by INGV. In this paper, we will refer to the Gargano Seismic Network (hereafter GSN) as to a network for the seismic monitoring of the GP area that includes 11 selected stations of the OT network and 10 selected stations of the IV network (Fig. 2) resulting in a very dense network optimized for this study.

2.1 OTRIONS seismic network (OT)

In 2013, the OTRIONS (multi-parametric network for the study and monitoring of natural hazards in the OTRanto channel and IONian Sea) project was funded in the context of the “European Territorial Cooperation Programme Greece-Italy 2007-2013” (INTEREG III) and one of the goals was to deploy a local seismic network around the GP (Tallarico, 2015). The first configuration of the OTRIONS seismic network, refers to years 2013-2014, consisted in 12 seismic stations in the Gargano Promontory: OT01, OT02, OT03, OT04, OT05, OT06, OT07, OT08, OT09, OT10, OT11, OT12. In June 2015, OT01, OT02, OT08 and OT09 were disabled and two new stations installed in the North of the area to provide a better coverage of the Northern part of the GP (OT13 and OT14 respectively). OT10 was disabled in 2019 due to technical problems. In 2021, two seismic stations were added (OT16 and OT17) . In Fig. 2 the actual OT network is shown, where the blue triangles refer to the active recording stations and black triangles refer to disabled stations.

In order to detect eventual electromagnetic signals related to seismic activity in GP, the station OT04 hosts, since September 2021, a magnetotelluric sensors as described by Ventola et al. (2024). In April 2024, 5 OT stations (OT05, OT11, OT12, OT14, OT16) have been renewed by changing the short-period Lennartz 3D-Lite (1s) seismometers with a broadband sismometer Nanometrics Trillium Compact (20s). The station OT11 was integrated with a Nanometrics Titan accelerometer in the same manhole where the broadband sismometer is housed. Moreover, in the same station has been added a co-located station (OTP1) equipped with a broadband posthole seismometer (Nanometrics T120s-PH3) in a 30 m deep well, providing the simultaneously

© Author(s) 2025. CC BY 4.0 License.

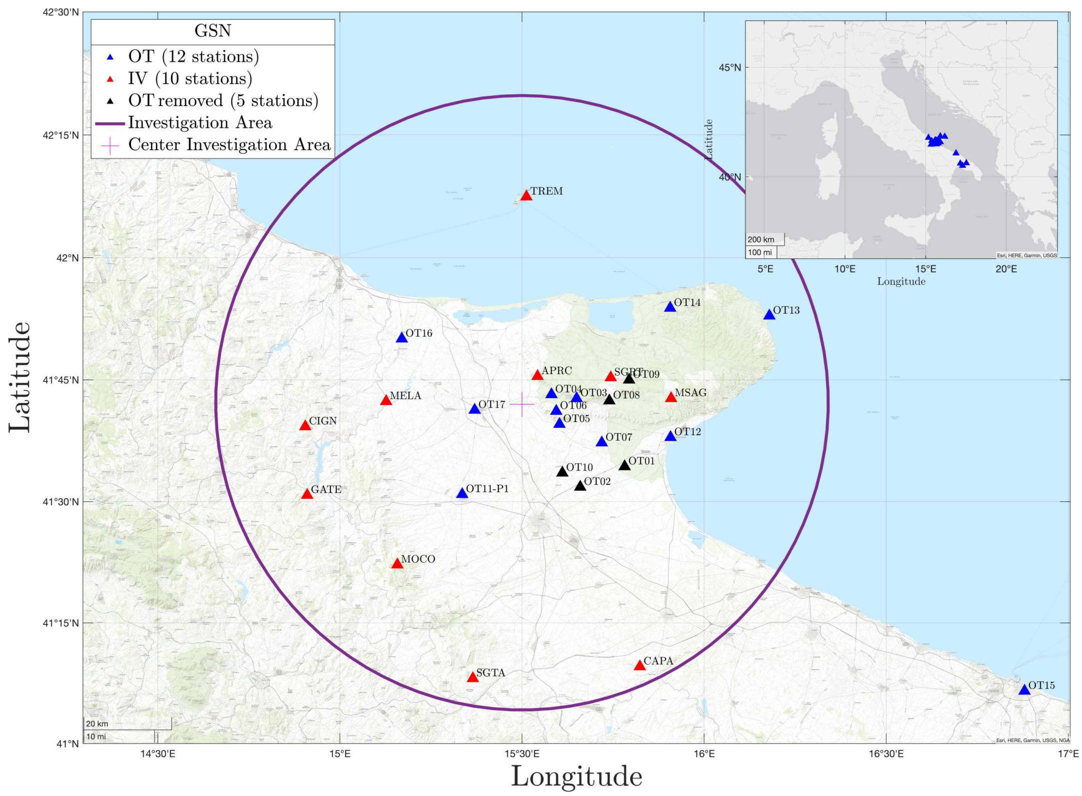

Figure 2. GSN network (blue, red and black tringles, explained in the figure legend) and the investigation area (purple cirle). The center of the investigation area(red cross) is [15.5E; 41.7N] with radius of 70 km

recording of seismic signal at the surface and at depth, useful for the orientation of the posthole sensor (details of the installation and of the sensor orientation are described by Tallarico et al. (2025)). All OT stations, are real time connected to RSN (INGV) by LTE or/and satellite connection. Regarding IV stations of the GSN (red triangles in Fig. 2), TREM from 2017 experienced heavy problems in the internet connection solved only in 2020.

The network performance was evaluated by comparing the expected working days with the actual days of operation for each station. Results are shown in Tab. A1 for each year from 2013 to 2022. It is worth that, after the 2019, the performance of the OT network greatly improve respect to the preceding period. In fact, until the first half of 2019, the seismic recordings of the OT network were archived and managed by the seismic laboratory facilities at UniBa; as a consequence, many technical and connection issues affected several stations and the local server causing data gaps. In order to solve these problems, thanks to a collaboration with INGV, after the 2019, data collection, transmission and repository have undergone a major technological improvement which allowed the transition to EIDA (European Integrated Data Archive, https://www.orfeus-eu.org/data/eida/ accessed on 30^{th} May 2025), witnesses by the meaningful improvement of OT performance. Conversely, the IV network shows

https://doi.org/10.5194/essd-2025-335
Preprint. Discussion started: 11 July 2025
© Author(s) 2025. CC BY 4.0 License.

consistently better performance over time in relation to the civil protection purpose of the network itself (Tab. A1 in the section A).

2.2 Seismic noise of the OT network

Quantifying the background seismic noise recorded by a seismic station is important to assess the quality of a registration site and the operational status of the seismic station. The standard method used to evaluate the background seismic noise is the calculation of the Power Spectral Density (PSD) of the seismic station recordings and its Probability Density Function (PDF). We have computed the PDF of the OT stations with Obspy, the Python tool for seismology (Krischer et al. 2015). The function is based on the algorithm of McNamara and Buland (2004), which calculates the Probabilistic Power Spectral Densities (PPSDs), that is the probability of having a certain noise level in a given period.

In the period $2013-2022$ the present catalog refers to, the OT network was composed of three-component short-period Lennartz 3D-V seismometers, with a flat response above 1 Hz and data loggers 24-bit SL06/SARA with dynamic range equal to 124 dB sampled at 100 Hz (Tallarico et al., 2025). Fig. 3 shows the PPSDs relative to the vertical component of six stations. We computed the PPSD of the continuous data stream recorded by any station for 7 days. The color palette shows the probability of the corresponding noise level at that period. The two gray curves show the high-level and low-level noise models of Peterson (1993). The horizontal bar below each PPSD panel shows, in the first row, the data availability in the considered week (green) or the data gaps (red), whereas in the second row the blue color indicates that each PSD (1-hour time series segment) has been considered in the computation of the PDF. The panel shows the values of PDF starting from the period of 0.02 s, which correspond to the Nyquist frequency $f_{Nyquist} = 50$ Hz, one-half of the station sampling frequency.

All of the short-period sensors show a dramatic increase of the noise level at periods greater than about 2 s, and at about 10 s, the noise is greater than the high-noise model, as a result of the instrumental self-noise at lower frequencies. We, therefore, focus on the noise level above 1 Hz (that is below 1 s). The noise level is optimal for most stations of the OT network, being the PPSD values located on the downside of the high-level noise (Peterson, 1993) model. In Fig. 3 from a) to c), the stations OT01, OT03 and OT08 record very good signal, having a PPSD centered between the high- and low-level noise models with small variations of the noise level (about 10 dB) at periods less than 1 s. Some stations, such as OT10, OT13, OT17, in Fig. 3 from d) to f), show higher values of cultural noise in the period range of 0.1-1 s. These stations are installed near state country roads (OT10) or in a city (OT13 and OT17), and probably suffer from the automobilistic traffic or machinery vibrations. Unfortunately some stations of the OT network (OT01, OT02, OT08, OT09) are no longer operational, and their high quality signals are even more valuable, suggesting that the recording sites are good for future installations. In the section A we released the PPSDs of the three-components for the entire OT stations of GSN.

3 Data analysis

The data used by CASP are the three components daily $(24h)$ recordings in miniSEED format. As already explained in Subsection 2.1, the $24h$ recordings of the OT network are available online since May 2019. For the preceding period, from April

© Author(s) 2025. CC BY 4.0 License.

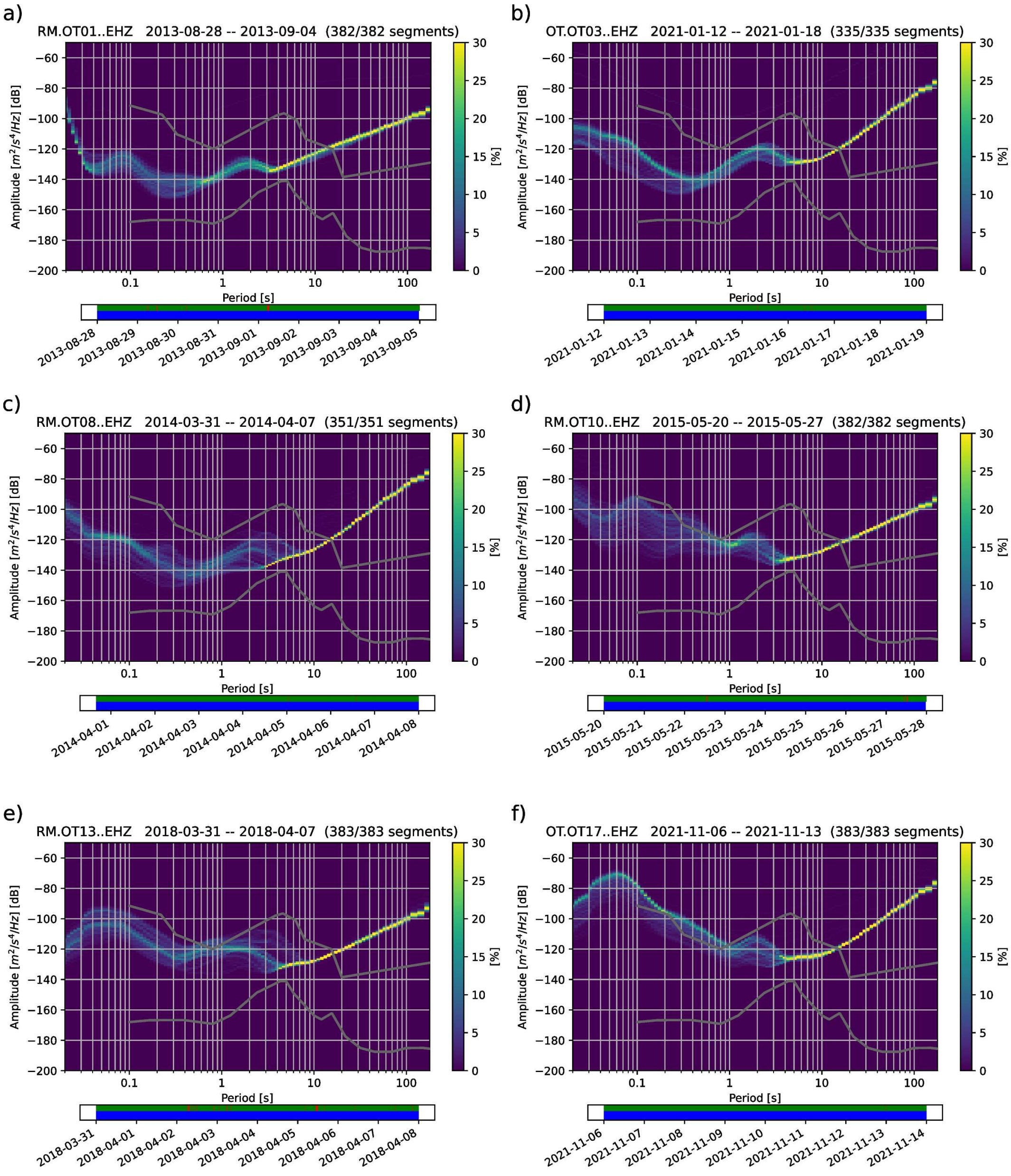

Figure 3. PPSDs of some vertical components of OT stations in dB. The name of the seismic station and the selected period of time is on the top. The color palette on the right shows the probability of the noise level. The horizontal bar below the panel shows the data availability or the data gaps (top row, green or red, respectively) and the PSD of each 1 hour time-series used for the probability calculation (bottom row, blue). The network code “RM” refers to the out-of-date name of the OT network.

https://doi.org/10.5194/essd-2025-335
Preprint. Discussion started: 11 July 2025
© Author(s) 2025. CC BY 4.0 License.

2013 to April 2019, we used the $24h$ recordings archived in the seismic laboratory of UniBa and available under request. So the dataset of $24h$ recordings, covering a period from April 2013 to December 2022, was collected as follow:

- from April 2013 to April 2019: recordings of OT stations were available in the seismic laboratory at UniBa; recordings of IV stations were downloaded from the INGV web-service (https://eida.ingv.it/en/ accessed on 30^{th} May 2025);
- from May 2019 to December 2022: recordings both of OT and IV stations were downloaded from the INGV web-service (https://eida.ingv.it/en/ accessed on 30^{th} May 2025);

The OT stations used are indicated in Tab. 1 with the corresponding locations. The operation period and instrumental characteristics are explained by Tallarico et al. (2025) . Seismic daily recordings were analyzed by the CASP software that provides a list of seismic events (further details can be be found in the Subsection 3.1). In order to ensure a high quality catalog and to evaluate the reliability of the results of CASP, we manually revised the automatic list of events (AL) in order to recognize 3 categories as labeled so far:

- EQ = Earthquakes inside the investigation area
- QB = Quarry Blasts
- FB = False events and/or bad located earthquakes

Hereafter, we detail the procedure to obtain the final catalog.

https://doi.org/10.5194/essd-2025-335
Preprint. Discussion started: 11 July 2025
© Author(s) 2025. CC BY 4.0 License.

Station	Name	Latitude	Longitude	Altitude (m)
CGL1	Ceglie Messapica	40.648	17.517	303
MASS	Massafra	40.633	17.144	274
OT01	Monte Aquilone	41.572	15.782	128
OT02	SS 89 km - Private Address	41.53	15.66	39
OT03	Pro Civ - San Marco in Lamis	41.712	15.650	655
OT04	Stignano - San Marco in Lamis	41.720	15.581	279
OT05	Rignano Garganico	41.659	15.603	180
OT06	Rignano Garganico	41.686	15.594	584
OT07	San Giovanni Rotondo - Pozzo Costarelle	41.621	15.719	154
OT08	San Giovanni Rotondo - Cemetery	41.707	15.739	581
OT09	Caserma Guardaboschi	41.750	15.794	846
OT10	Borgo Arpinova	41.559	15.611	64
OT11	Lucera	41.515	15.336	214
OTP1	Lucera	41.515	15.336	214
OT12	Manfredonia	41.632	15.908	30
OT13	Vieste	41.881	16.1791	33
OT14	Ischitella	41.897	15.907	401
OT15	Bari	41.109	16.880	16
OT16	Chieuti	41.834	15.170	256
OT17	San Severo	41.688	15.370	91
TAR1	Taranto	40.526	17.285	71

Table 1. Stations of the OT network with name and location.

3.1 CASP automatic list of events - AL

CASP is an advanced software for the detection, picking and automatic location of seismic events (Scafidi et al., 2019) written in standard C programming language. The architecture of this software consists of four main modules.

– The first module is the *Trigger* and it generates a list of triggers by applying the STA/LTA (Short Term Average/Long Term Average) algorithm on the vertical component of each station recording. In this step, to ensure the best balance between signal noise and trigger sensitivity, the optimal STA and LTA values were defined through a series of preliminary tests conducted over a dataset of 100-day's recordings. An appropriate $\mathrm{STA/LTA} = 0.8/25$ and filtering (band pass filter between 10 Hz and 25 Hz), based on these tests, was selected as best choice.

https://doi.org/10.5194/essd-2025-335
Preprint. Discussion started: 11 July 2025
© Author(s) 2025. CC BY 4.0 License.

- The second module is the *Detect* for trigger association and event detection and it analyzes the list of triggers to associate traces and identify the possible seismic event.
- The third module is the *Extract* for extraction of time windows including potential earthquake and it works, if an event is detected, by converting seismograms into SAC format and by creating an event directory.
- The fourth module is the *Picker2* for picking of P- and S-arrival times and for event location and magnitude. It performs the automatic P- and S-phase picking working on the event directory, provides the locations by using NLL (Lomax et al., 2000) and computes the magnitude with the procedure adopted in Spallarossa et al. (2002) and the attenuation law of Di Bona (2016). This modular sequence enables a fully automatic processing of the $24h$ recordings resulting in an automatic list of events, as fully described by Scafidi et al. (2018) and Scafidi et al. (2019). In this module configuration, the $PostSTeo$ parameter, maximum time interval between the P-wave and S-wave picks, was set to a value determined through several tests, which demonstrated the sensitivity of event detection to this parameter. The optimal value for our study area is $PostSTeo = 5$ s. The velocity model implemented was already used for the GP seismicity (Miccolis et al., 2021, and reference therein). The NLL location grid was set with a node spacing of 1 km both in latitude and longitude. This spacing allows optimal resolution in the location of the seismic events, ensuring an accurate representation of hypocenters within the investigation area. To study in detail the seismicity of the GP area and taking into account the geometry and density of GSN, we defined a circular investigation area shown on map as a purple circle, with 70 km radius and center in $(15.5\mathrm{E}; 41.7\mathrm{N})$ (Fig. 2). Th results of this sequence of CASP modules, applied to the database of ten years registrations, is an automatic list of 6915 events that we decided to manually revise.

3.2 Manual revision of the automatic list

The analysis of the automatic catalog revealed several critical issues that negatively affected the quality and reliability of the events detected and located within the investigation area. The main issues encountered were associated to a number of factors like: the wrong location of seismic events outside the network, the reporting of false events and events with low-quality location. In order to address these issues, we manually revised the CASP automatic picking. A total number of 54205 seismograms were manually re-picked. With the manual revised P and S wave picks, we then proceeded with the relocations by using the NLL code (Lomax et al., 2000).

3.2.1 False and bad-located event - FB

In Fig. 4, an example of a false event recorded at three different stations, picked and located by CASP and so wrongly considered as a seismic event, is shown. All the events recognized as false were discarded.

https://doi.org/10.5194/essd-2025-335
Preprint. Discussion started: 11 July 2025
© Author(s) 2025. CC BY 4.0 License.

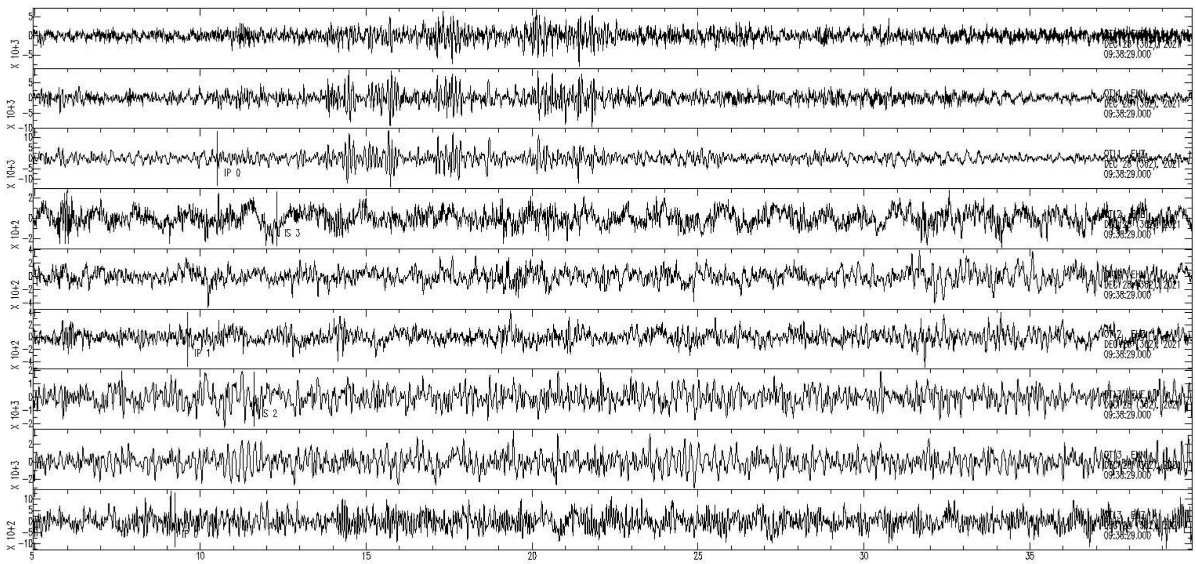

Figure 4. Example of false event picked by CASP. Three component registrations at station OT11, OT12 and OT13 are shown together with pick markers of P (on the Z component) and S waves (on the E component) in SAC format. Vertical axes are "Velocity" in counts/sec; horizontal axis is "Time" in sec from the begin time indicated on the trace.

During the review of the automatic list of events, we recognized some errors that led to very bad locations. In Fig. 5 an example of erroneous picking of the S wave is shown, due to an anticipation of the recognition of the arrival of the S wave, constrained to be searched a few seconds after the recognition of the arrival of the P wave, through the setting of the $PostSTeo$ parameter. If the error is repeated on more than three stations, the consequence is that the event is associated and detected as belonging to the GP area, even though it is an earthquake hundreds of kilometers away from the investigation area, as verifiable by a comparison with the earthquake list of the ONT (National Earthquake Observatory, INGV). The event in the Fig. 5 is an ML 2.3 on 13-07-2016 at 20:53:42 (UTC) in an area at few dozen kilometers from the edge of the investigation area. In the automatic list of events, we recognized 2012 false and bad located events, all due to erroneous S-wave picking, corresponding to the 29% of the total. All these events were discarded.

4903 seismic events of the initial 6915 can be classified as seismic events, corresponding to the 71%.

3.2.2 Quarry blasts - QB

A separate discussion must be addressed for the explosions in the quarries. In the Apulian territory there are 399 active quarries divided in four production mining basin and the mining activity guaranteed throughout the year, thanks to climatic conditions and to the presence of a cutting-edge transformation and processing industry. The GP area produces 90% of the total stone materials extracted in the Apulia region and 20% of the Italian one, then it is the most important in southern Italy (a detailed description can be found at the institutional website of Apulia region (http://eventi.internazionalizzazione.regione.puglia.it/

https://doi.org/10.5194/essd-2025-335
Preprint. Discussion started: 11 July 2025
© Author(s) 2025. CC BY 4.0 License.

Open Access Earth System Science Data Discussions

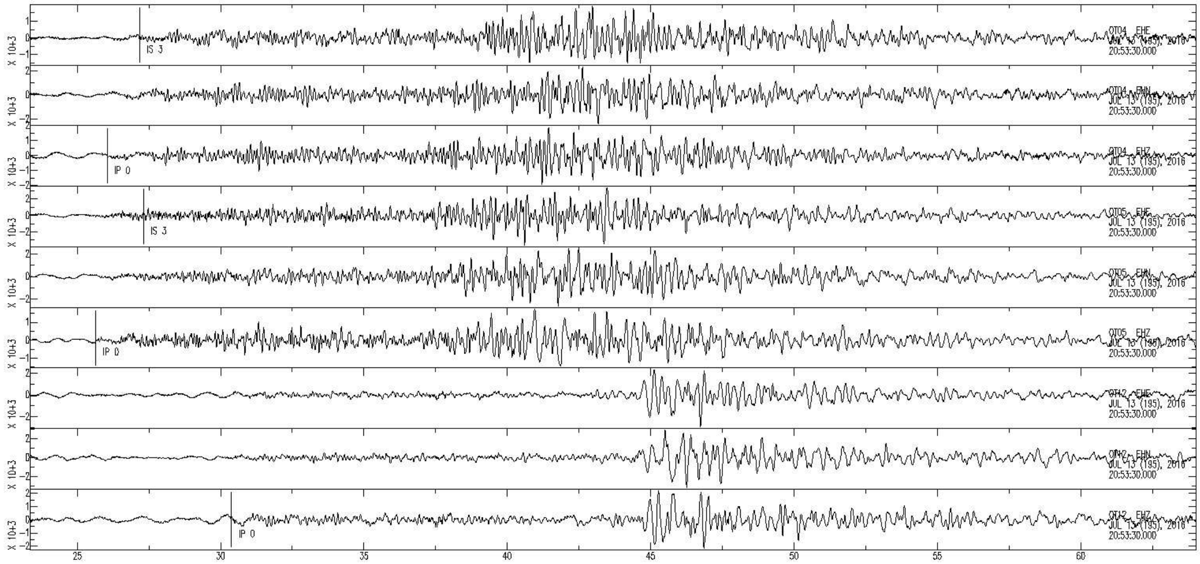

Figure 5. Example of bad picking. The three component seismograms at stations OT04, OT05, OT12 with the corresponding picking of P waves (on the Z component) and S waves (on the E component) are reported in SAC format. Vertical axes are "Velocity" in counts/sec; horizontal axis is "Time" in sec from the begin time indicated on the trace.

web/guest/materiali-lapidei). In the GP mining basin the famous shallow-water limestone (Festa et al. (2016) and reference therein) known as *Apricena stone* is extracted, one of the most appreciated in the world for its beauty and versatility. This intense mining activity can be recorded by local and dense seismic network since the magnitude of blasts can reach M_L up to $2.5-3.0$ in Europe and up to 4.0 in USA (Gulia, 2010). We recognized several hundred events probably caused by explosions in quarries to be examined. In the histogram in Fig. 7, the 4903 seismic events subdivided per daily hours, indicates that a great part of them occurs during daily time, when the seismic noise is higher and the seismic detect should be lower, so we can suspect that the source is anthropogenic. The identification of these events, reported as QB = Quarry Blast, was obtained in different phases. First, we made a comparison with the quarry blasts recognized by the ONT bulletin, where the labeling of quarry explosions has recently been inserted. This comparison is not enough because the discrimination between tectonic earthquakes and anthropogenic events suffers from some problems of data processing and so artificial seismicity may be present in the ONT earthquake catalogue, thus invalidating any physical or statistical interpretation using the earthquake catalog data (Gulia and Gasperini, 2021). Then we collected a subdataset by selecting those events that:

- occurred on weekdays, from Monday to Friday;
- occurred in a UTC time between 07:00:00 and 18:00:00;
- having an hypocentral depth within 5 km, then extended to 10 km;

https://doi.org/10.5194/essd-2025-335
Preprint. Discussion started: 11 July 2025
© Author(s) 2025. CC BY 4.0 License.

– located in the coordinate ranges corresponding roughly to the areas in which the aforementioned quarries are present and authorized to the use of explosives (by consulting a database provided by Apulia district).

No magnitude filter was used since the events in the automatic list have magnitude $M_L < 3$ for the vast majority. In a later and final phase, we visually inspected the seismograms of the selected subdataset to identify the explosions. In Fig. 6 an example recordings of identified blast is shown.

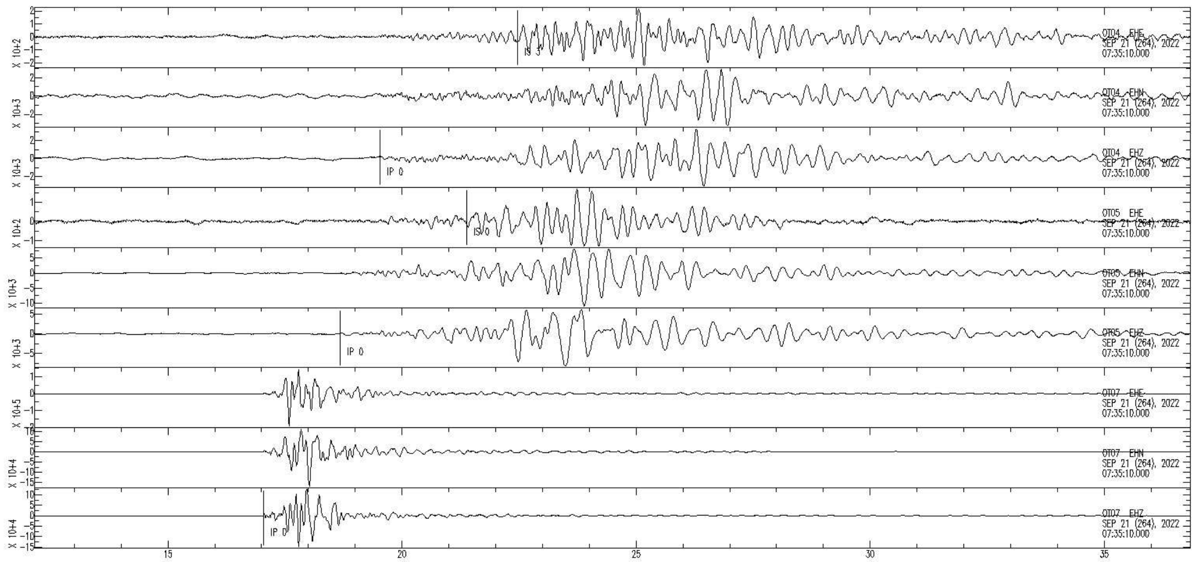

Figure 6. Example of quarry blast registration. The three component seismograms at stations OT04, OT05, OT07 with the corresponding picking of P waves (on the Z component) and S waves (on the E component) are reported in SAC format. Vertical axes are "Velocity" in counts/sec; horizontal axis is "Time" in sec from the begin time indicated on the trace.

We recognized 776 explosions as shown on satellite orthophotos (yellow dots in Fig.7a) where some clusters are clearly visible in correspondence with quarries for which the use of explosives is authorized. The explosions outside the clusters can be ascribed to survey activities by blasts. After removing the 776 quarry blasts, 4098 seismic events can be labeled as natural earthquakes (blue dots in Fig.7a). In Fig. 7b the histograms of the number of earthquakes subdivided per daily hours is shown indicating a pattern coherent with the tectonic activity and seismic noise in agreement with the results of Gulia (2010) for northern Italy. It is worth to note that, if we do not remove QB from the catalog, the interpretation tectonics of the GP from the seismicity patterns can be strongly biased. In fact in Fig. 7c it can be observed that quarry blasts in our GP catalog brings to identify a fictitious shallow seismogenic layer between 3 and 7 km.

https://doi.org/10.5194/essd-2025-335
Preprint. Discussion started: 11 July 2025
© Author(s) 2025. CC BY 4.0 License.

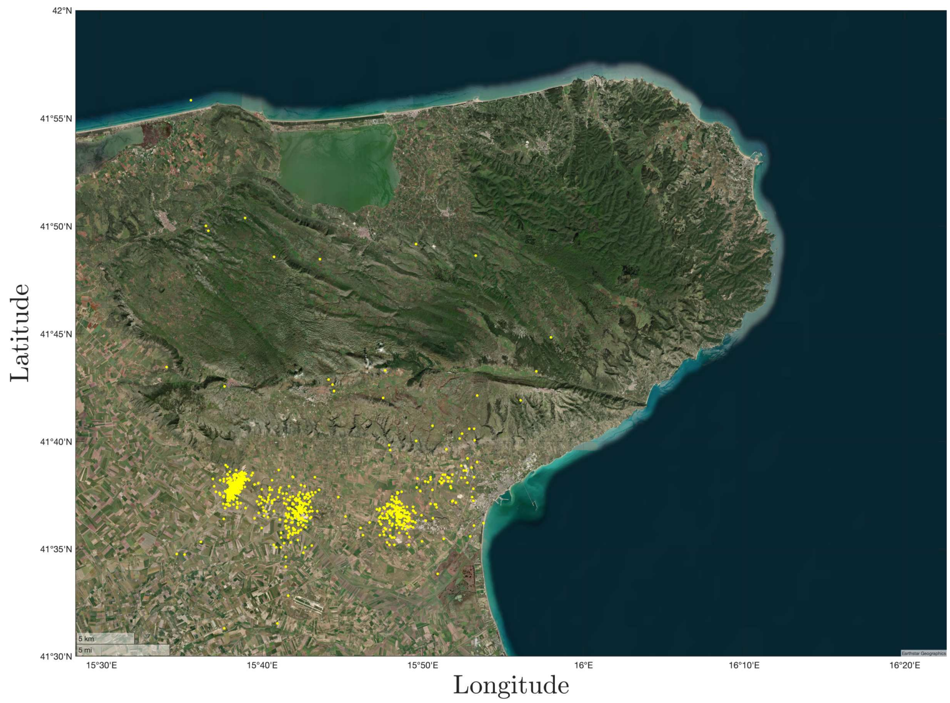

(a)

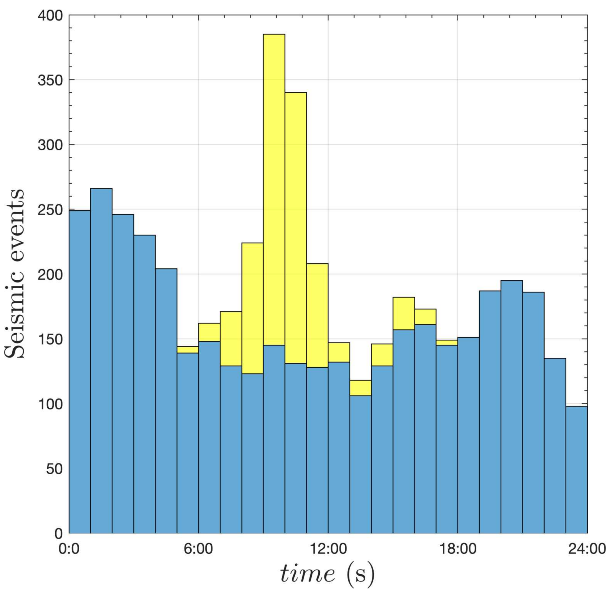

(b)

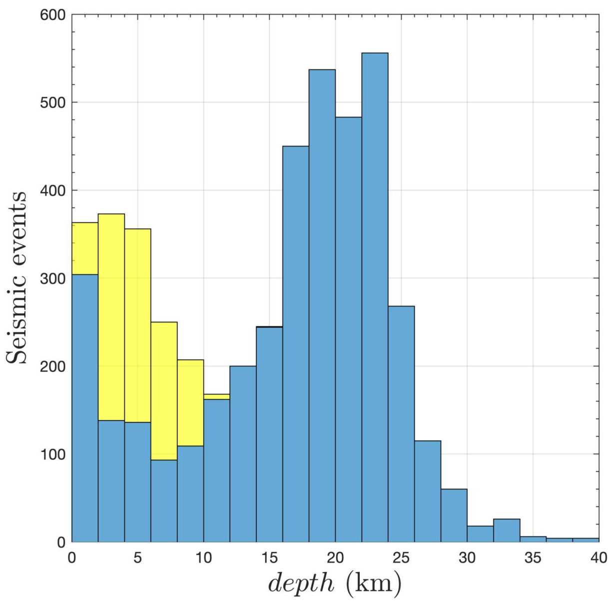

(c)

Figure 7. a) Map of QB epicenters. b) Daytime histograms of EQ and QB, c) depth histograms of EQ and QB. Yellow color in the hystograms and in the map refers to QB events. Blue color in the histograms refers to EQ events. The map was created in Matlab by MathWorks®

https://doi.org/10.5194/essd-2025-335
Preprint. Discussion started: 11 July 2025
© Author(s) 2025. CC BY 4.0 License.

Event type	Number of events	Percentage respect to AL
AL	6915	–
EQ	4098	60%
QB	776	11%
FB	2012	29%

Table 2. Results of the revision of the automatic list (AL) of events. Acronyms are explained in section 3. The number of events for each event type and the relative percentage respect to the total number of events present in the automatic list AL is reported

At the end of the manual revision of the automatic event list, we obtained the results shown in Tab. 2. The result indicates that the rejected events are the 40% of the automatic list highlighting that manual revision of picking is necessary to ensure the reliability of the seismic catalog.

4 CASP automatic vs manual picking

A comparison between the automatic and manual picking of only EQ events was performed. The differences between the manual and the automatic picking of the arrival times of P waves ($\Delta T_P = T_{P_M} - T_{P_A}$, with T_{P_M} and T_{P_A} the P wave manual and automatic picks respectively) and S waves ($\Delta T_S = T_{S_M} - T_{S_A}$, where T_{S_M} and T_{S_A} are the S wave manual and automatic picks respectively) are evaluated, obtaining the results shown in Fig. 8. It can be observed, that for P waves the average $\overline{\Delta T_P} = 0.047$ s indicates a slight systematic error on picking while the standard deviation $\sigma_{\Delta T_P} = 0.267$ s indicates a small dispersion of ΔT_P. $\overline{\Delta T_P} > 0$ indicates that the majority of the automatic picks are ahead with respect to manual ones. Differently for S waves, $\overline{\Delta T_S} = 0.106$ s indicates a greater systematic error on picking, picks are more ahead in a greater extent with respect to manual ones and with a great dispersion ($\sigma_{\Delta T_S} = 2.586$ s). The major dispersion of time picking differences is for ΔT_S and indicates that the module *Picker2* better identifies P-wave than S-wave arrivals but the asymmetric left distribution shown in Fig. 8 indicates that the automatic arrival times are systematically underestimated and this could affect event location bringing the event closer to the network than it should be, as described in section 5.1.

5 Earthquake catalogs of GP

Once selected the 3948 EQ from the automatic event list, the relocation with the manually reviewed arrival times of P and S waves was performed and the evaluation of the location quality was assessed. We decided to compare the location results obtained by both a linearized location algorithm ($H71$ by Lee and Lahr (1975)), used in the preceding catalog of the GP area (Filippucci et al., 2021; Miccolis et al., 2021) and a non-linear location algorithm (NLL by Lomax et al. (2000)) used also by $CASP$. Comparisons between linearized and non-linear localization methods are not very numerous in the literature. Considering the comparison between location methods that use 1-D velocity models (Lomax et al., 2000; Presti et al., 2008) the

© Author(s) 2025. CC BY 4.0 License.

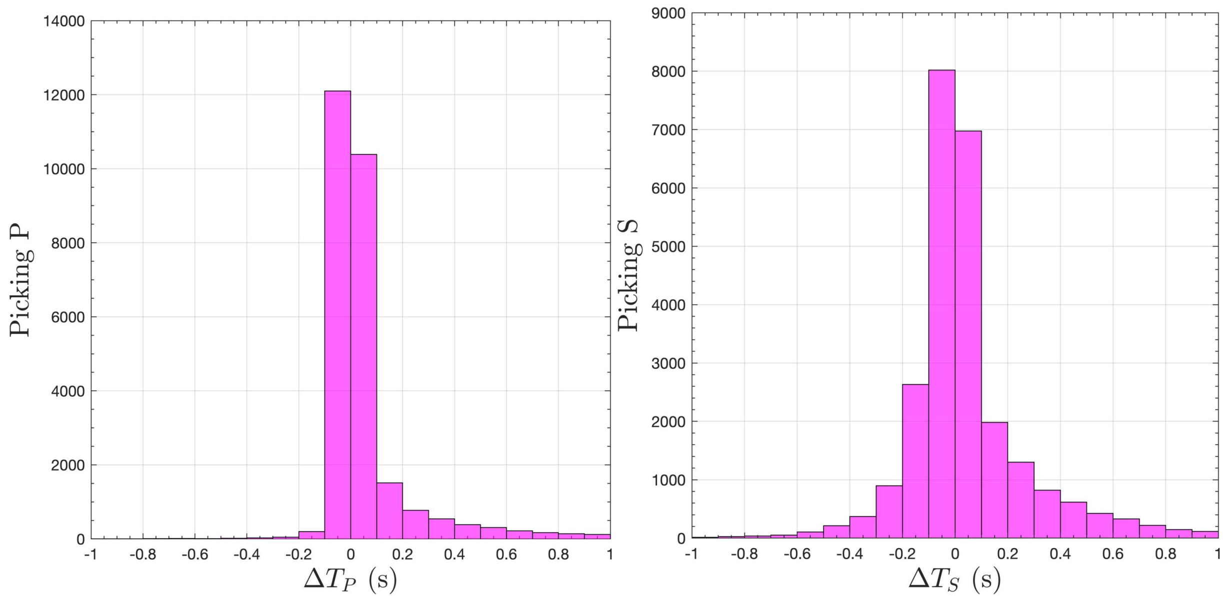

(a) (b)

Figure 8. a) Histogram of the number of P arrival time's pickings; b) histogram of the number of S arrival time's pickings.

results about both hypocentral coordinates and localization errors indicate that a non-linear approach is generally preferable and leads to more reliable results especially when the problem is not well conditioned and the location probability in the space-time domain belongs to an undefined large volume. Otherwise, when the network coverage around the earthquakes is quite good, the errors on picking of P and S time arrivals are small and a crustal velocity model is adequate, the linearized localization method gives locations of comparable quality to those of non-linear methods (Abbasi, 2019).

5.1 NLL-catalog of EQ

To asses the accuracy and robustness of a seismic localization, one can employ estimators. For NLL, these might include 8 uncertainty parameters for location, organized in the histograms in Tab. 3. The uncertainty parameters are:

- rms: root mean squared travel-time residuals;
- erh: horizontal error on epicenter location;
- erz: vertical error on hypocenter location;
- $nphs$: number of P and S phases used for location;
- gap: azimuthal gap that is the largest angle between two receivers as seen from the epicenter;
- $dmin$: distance between the epicenter and the closest station of the network;

https://doi.org/10.5194/essd-2025-335
Preprint. Discussion started: 11 July 2025
© Author(s) 2025. CC BY 4.0 License.

- $locdist$: distance in km between the $expected$ value of the probability density function (pdf) of the hypocenter location (expressed as latitude lat_e, longitude lon_e and depth $depth_e$) and its maximum likelihood (expressed as lat, lon, $depth$);
- $rpdf$: radius in km of the volume V described by the scatter points.

The indicators $locdist$ and $rpdf$ are computed "a posteriori" as following (Lomax et al., 2009):

$$locdist = [(lat_e - lat)^2 + (long_e - long)^2 + (depth_e - depth)^2]^{1/2} \tag{1}$$

$$rpdf = \left[V \frac{3}{4\pi}\right]^{1/3}. \tag{2}$$

The uncertainty parameters are distributes over asymmetric statistics with maximum frequency on the statistical mode ν that is reported in Tab. 3 together with other statistical parameters. rms refers to location quality in the time domain and its statistics (mean median and mode) suggest an overall good quality; erh and erz refer to location quality in the space domain and their statistics show that the majority of the locations are characterized by low hypocentral errors; the number of phases $nphs$ used for location changes significantly showing the variability in the input travel times' dataset. All the indicator of locations are of good quality except for gap, the azimuthal gap indicator. gap, is the major issue in the GP area because of the geographical configuration of the Gargano promontory, which elongates in E direction toward the Adriatic sea. This causes an high angle of network uncovering which makes locating earthquakes in this area as difficult as locating events offshore . The gap (Fig. 9e) shows values distributed quasi-symmetrically around an average $\overline{gap} = 223°$, which is a very high value. If we would filter the earthquake database considering as quality criterion $gap < 240°$, as already done in the previous earthquake catalogs of GP (Filippucci et al. (2021),Miccolis et al. (2021)) we should reject almost half of our database. Being a criterion based on gap too restrictive for the peculiar GP area, we evaluated the quality of earthquake location by following an approach similar to that of Michele et al. (2019). Results are in subsection 5.3.

A total of 4098 earthquakes were located and these locations were compared with those provided by the CASP automatic procedure. In Fig. 10, the differences between the epicentral position (Δepi), hypocentral depth ($\Delta depth$) and origin time ($\Delta orig$) are shown. The statistical distributions are Gaussian and centered on approximately zero ($\overline{\Delta epi} = 4.9 \pm 13.0$ km; $\overline{\Delta depth} = 0.82 \pm 6.7$ km; $\overline{\Delta orig} = -0.56 \pm 2.54$ s) suggesting that systematic differences are negligible. Standard deviation on epicenter position difference, $\sigma_{\Delta epi} = 2.2$ km, is less then the half average horizontal error $\overline{erh} = 2.74$, $\sigma_{\Delta depth} = 4.0$ km is comparable with the average vertical error $\overline{erz} = 4.54$ km and $\sigma_{\Delta orig} = 0.3$ s is comparable with $\overline{rms} = 0.18$ s indicating a good agreement between manual and automatic location of epicenter and origin time.

From this analysis it appears that the major issue related to the CASP automatic detection is the recognition of the event type, if it is a regional event, a false event or a quarry blasts and a lot of human resources work is needed in selecting the event type from the automatic detect list, as described in Section 3.2. Differently, on the selected earthquakes EQ, the automatic location system implemented in CASP doesn't need a manual revision, as shown in Fig. 10.

https://doi.org/10.5194/essd-2025-335
Preprint. Discussion started: 11 July 2025
© Author(s) 2025. CC BY 4.0 License.
Open Access Earth System Science Data Discussions

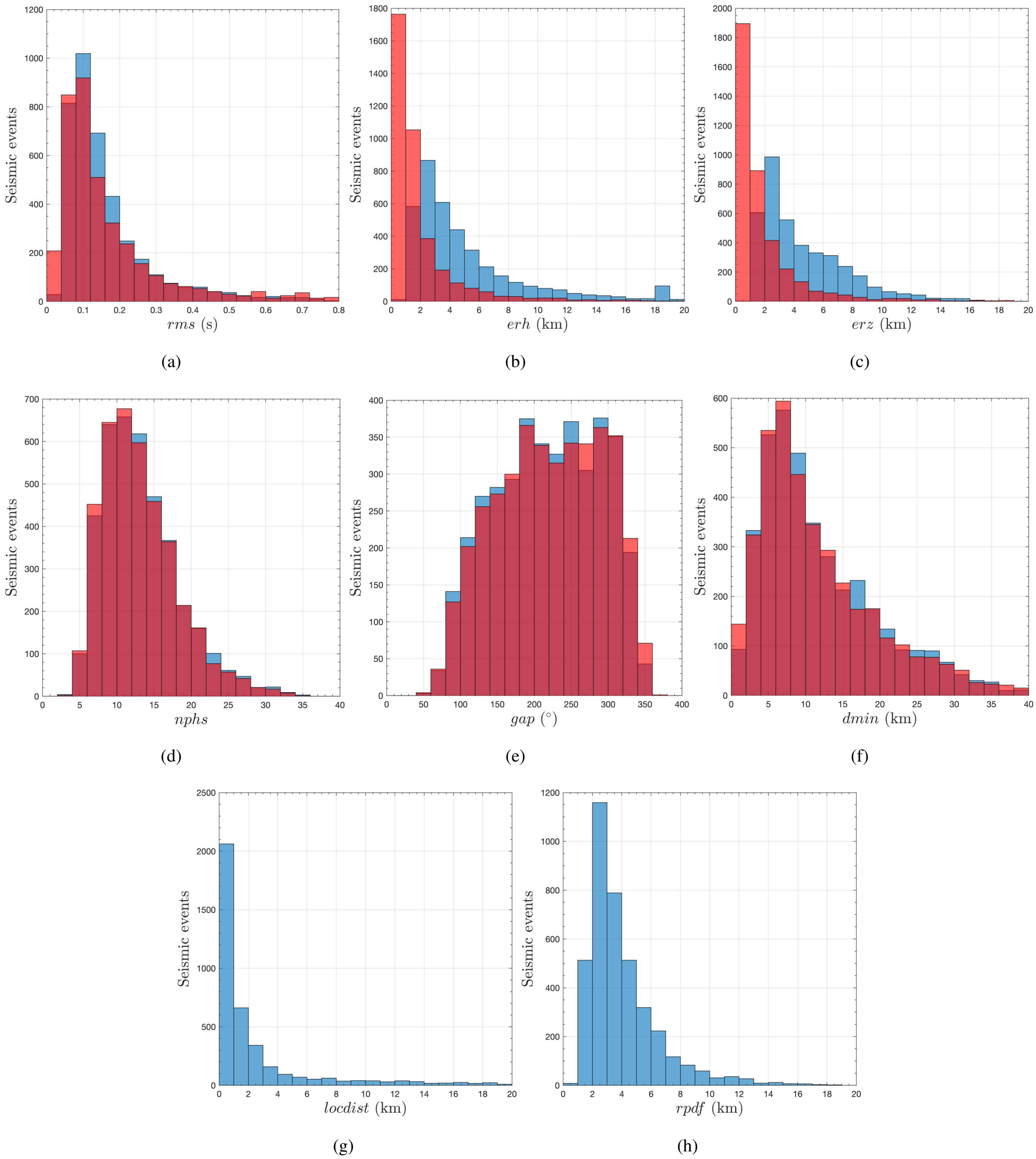

Figure 9. Histograms of quality location estimators for the H71-catalog (orange) and NLL-catalog (blue) and the overlapping areas (red).

https://doi.org/10.5194/essd-2025-335
Preprint. Discussion started: 11 July 2025
© Author(s) 2025. CC BY 4.0 License.

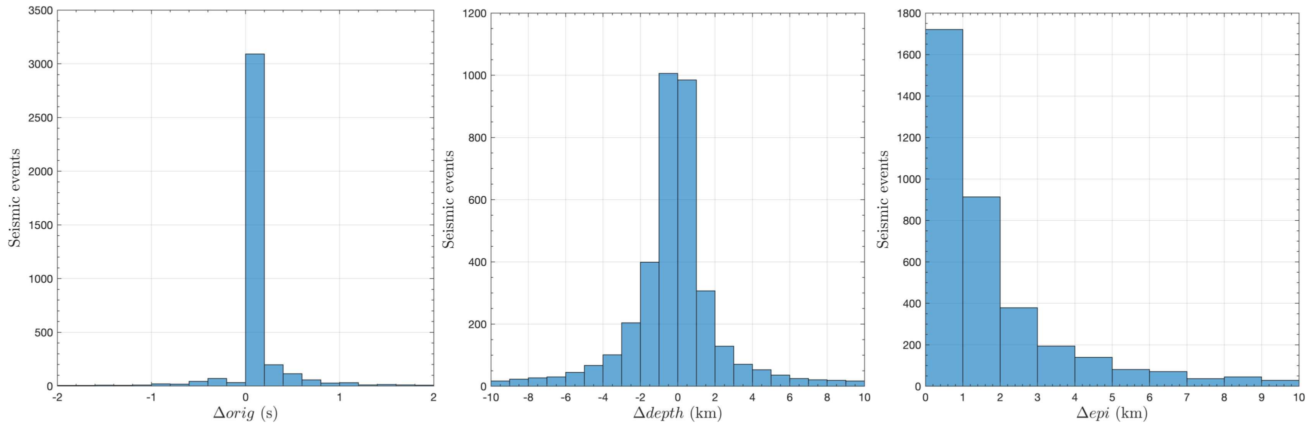

(a) (b) (c)

Figure 10. Histograms of the location difference between the automatic catalog and the NLL manual catalog.

5.2 H71-catalog of EQ

Deterministic location methods based on linearized inversion, as H71, start from an assumption on the initial hypocentral position. If the estimate of the initial position does not sufficiently match the true hypocenter, then the linearized solution may converge to a local minimum in the source parameter domain. This local minimum may differ substantially from the global minimum that should correspond to the exact hypocenter. In this paper, the initial value of the hypocentral depth has been refined using different initial depths (10 initial depths with a step of 10 km, starting from 10 km to a depth of 100 km) and the best location, among the 10 locations for each earthquake, has been selected through the minimization of the dimensionless parameter S (Miccolis et al., 2021):

$$S = \frac{rms}{rms_0} + \frac{erh + erz}{\sqrt{dmin^2 + depth^2}} \tag{3}$$

where $rms_0 = 1$ s is a reference residual time and $dmin$ is the distance between the epicenter and the closest station of the network. A total of 4105 earthquakes were located. The indicators of H71 location quality, listed in Tab. 3 and plotted as hystograms in Fig. 9 in orange color, are similar to those of NLL, except for the probabilistic estimators ($locdist$ and $rpdf$) that are not computed by linearized location methods. Results indicate an overall good quality of the linearized catalog, except for the azimuthal gap values, gap, as expected.

5.3 Quality of NLL-catalog and H71-catalog of EQ

Differences between the 2 catalogs are shown in Fig. 9 relatively to the quality indicators. It is worth to note that, by analyzing the 3 indicators rms, erh and erz, the quality of H71-catalog is overall better that that of NLL-catalog, with time/space uncertainties systematically lower. In Fig. 11 we showed 3 hypocentral depth histograms for each catalog with relative vertical error bars. At left we can see that the histogram of $depth - erz$ in the NLL catalog shows 550 earthquakes that could be located

https://doi.org/10.5194/essd-2025-335
Preprint. Discussion started: 11 July 2025
© Author(s) 2025. CC BY 4.0 License.

	NLL-catalog								H71-catalog					
	rms (s)	erh (km)	erz (km)	$nphs$ #	$dmin$ (km)	gap (°)	$locdist$ (km)	$rpdf$ (km)	rms (s)	erh (km)	erz (km)	$nphs$ #	$dmin$ (km)	gap (°)
mean	0.18	5.48	4.54	13	12.46	218	2.95	4.04	0.25	3.75	2.33	12	12.32	220
median	0.13	3.70	3.50	12	9.79	220	0.90	3.31	0.11	1.00	1.00	12	9.50	223
mode	0.06	2.10	2.20	10	8.50	331	0.03	1.69	0.07	0.50	0.50	10	0.20	249
50 perc	-	-	-	-	-	-	-	-	-	-	-	-	-	
90 perc	0.32	11.51	8.50	20	24.74	310	8.69	7.05	0.46	5.00	4.60	19	24.80	312
95 perc	0.45	16.91	10.50	6	29.66	323	14.15	8.99	0.72	8.70	7.50	6	30.20	327
max	23.05	85.00	17.00	35	84.73	358	72.79	22.68	19.09	619.90	129.30	35	85.20	360
min	0.01	0.70	0.00	3	0.24	55	0.02	0.82	0.00	0.70	0.00	3	0.20	51

Table 3. Statistical parameters (in the first column: mean (), median (m), mode (ν), 50^{th}, 90^{th} and, 95^{th} percentiles, maximum and minimum values) of the uncertainty estimators of the NLL and H71 catalogs.

several km above the Earth surface while in the H71-catalog this number is reduced to 98. This result indicates that for some hundreds of earthquakes the NLL locations of foci depth are of poor quality.

In order to quantitatively analyze and compare the quality of the two catalogs, the correlation matrices of both NLL and H71 uncertainty estimators are shown in Fig. 12. The great dispersion observed in the correlation plots indicates that correlation is weak thus the possible bias in earthquake locations is minimized.

We propose a quality parameter q_f for locations following that proposed by Michele et al. (2019). The q_f factor for each earthquake can be expressed by the following formula:

$$q_f = \left[w_1 \left(\frac{rms}{rms_n} \right)^2 + w_2 \left(\frac{erh}{erh_n} \right)^2 + w_3 \left(\frac{erz}{erz_n} \right)^2 + w_4 \left(1 - \frac{nphs - nphs_{min}}{nphs_{max} - nphs_{min}} \right)^2 + \right.$$

$$\left. + w_5 \left(\frac{gap}{gap_n} \right)^2 + w_6 \left(\frac{locdist}{locdist_n} \right)^2 + w_7 \left(\frac{rpdf}{rpdf_n} \right)^2 \right]^{1/2} {N_{est}}^{-1/2} \tag{4}$$

The subscript n means "normalized" to the 95^{th} percentile value present in the considered catalog, w_j is a weighting parameter ranging from 0 to 1 while the number j of indicators are $j = 7$ for NLL and $j = 5$ for H71. All indicators increase with decreasing location quality, except for $nphs$ for which we used as $nphs_{min} = 5^{th}$ percentile and as $nphs_{max}$ the maximum value of the considered catalog. Regarding the weights, we assumed $w_j = 1$ for all estimators, except gap where $w_{gap} = 0.5$.

q_f ranges from 0 (highest quality) to 1 (worst quality), and, based on this value, each earthquake falls into a quality class ranging from A (the highest quality) to D (the worst quality). The criteria for dividing q_f into the alphabetical quality classes are in Tab. 4. We used the 95^{th} percentile to normalize those estimators which increase with decreasing quality and we used the 5^{th} percentile to normalize the estimator (only $nphs$) that decreases with decreasing quality. This choice avoids to introduce outliers in the quality classes. With this criterion we discarded 160 earthquakes for H71 and 97 for NLL for which $q_f > 1$. At the end of this selection, the total number of earthquakes are $EQ = 3820$ for NLL and $EQ = 3782$ for H71. The quality

https://doi.org/10.5194/essd-2025-335
Preprint. Discussion started: 11 July 2025
© Author(s) 2025. CC BY 4.0 License.

Open Access Earth System Science Data Discussions

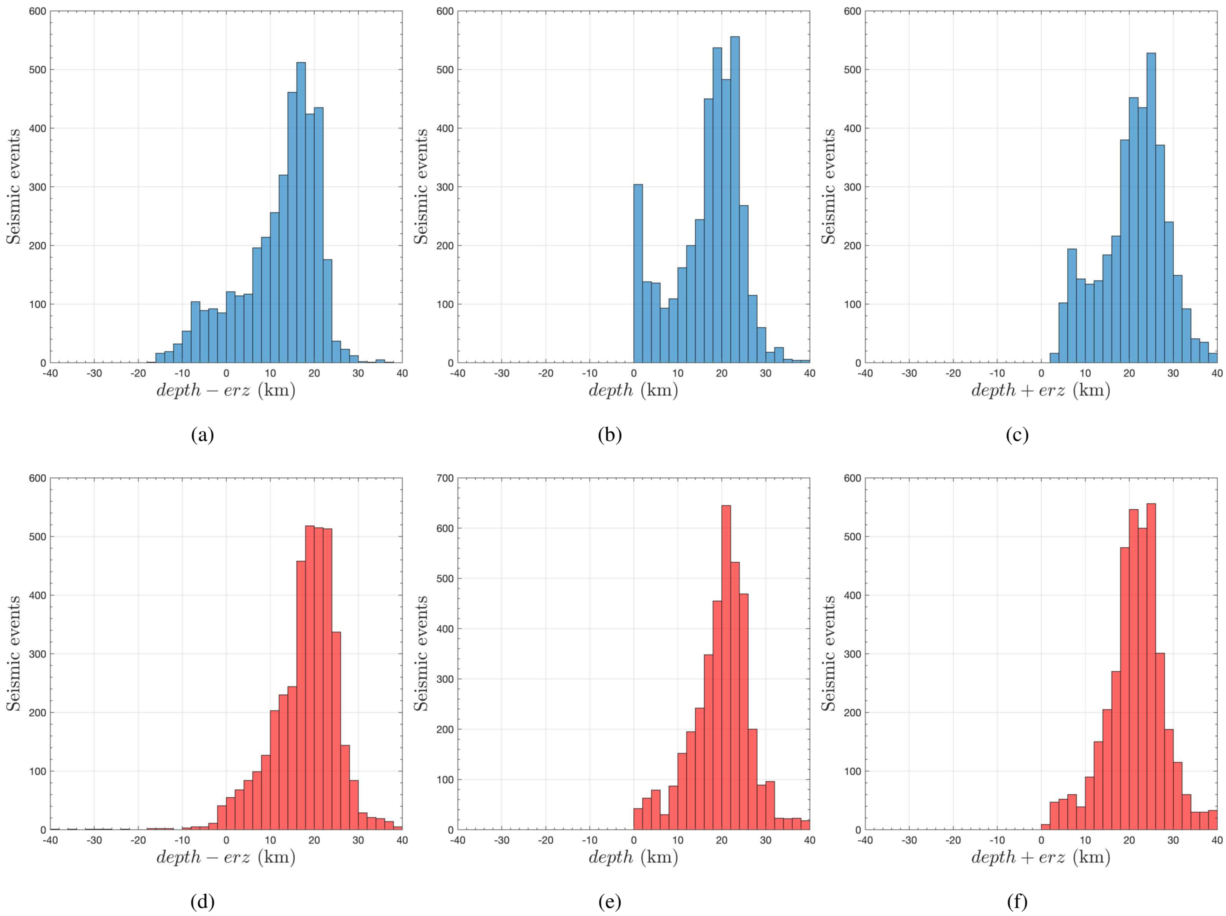

Figure 11. Histograms of differences between depth and associated vertical error for NLL-catalog (blue) and H71-catalog (red).

Quality class	q_f	EQ NLL-catalog	% EQ NLL-catalog	EQ H71-catalog	% EQ H71-catalog
A	$q_f \leq 0.25$	143	3.7%	219	5.8%
B	$0.25 < q_f \leq 0.5$	2490	65.2%	3093	81.8%
C	$0.5 < q_f \leq 0.75$	984	25.8%	437	11.6%
D	$q_f > 0.75$	203	5.3%	33	0.8%

Table 4. The 4 different quality classes for 4 evenly spaced intervals of q_f as adopted in Eq. 4 and the number of earthquakes that fall into each class with the percentage relative to the total number of earthquakes,

classes, reported in Tab. 4, indicate that most earthquakes fall into the 2 classes of B and C, for both the H71 and NLL catalogs. Earthquake locations on map are shown in Fig. 13 divided for quality class.

https://doi.org/10.5194/essd-2025-335
Preprint. Discussion started: 11 July 2025
© Author(s) 2025. CC BY 4.0 License.

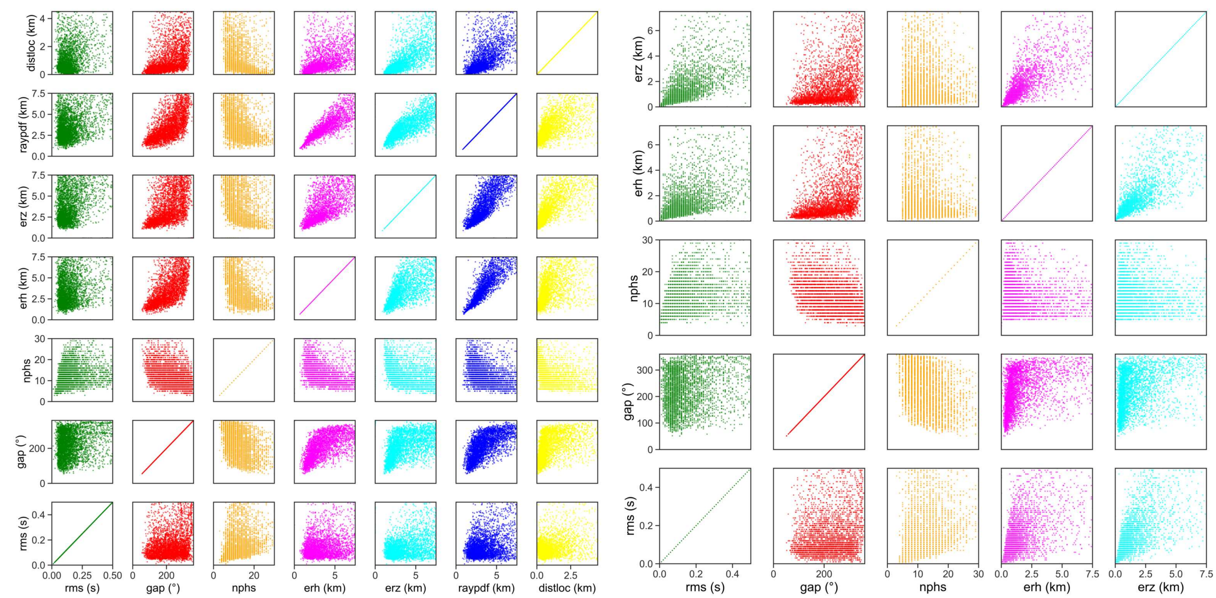

(a) (b)

Figure 12. Correlation matrices of the uncertainty parameters related to: a) NLL-catalog, b) H71-catalog.

5.4 Local Magnitude M_L

In the CASP procedure for location, the local magnitude M_L is also automatically calculated using the algorithm proposed by Spallarossa et al. (2002) for northern Italy. This procedure is included in the module *Picker2* where the configuration parameters are: the Butterworth pre-deconvolution low level filter (0.8–1.5 Hz), that cut the lower frequencies, the high level filter (30 Hz) that is lower than the Nyquist frequency, $f_{Nyquist} = 50$Hz, being 100 sps the sampling rate of the GSN, to avoid any aliasing effect. The module *Picker2* generates synthetic Wood-Anderson seismograms and calculates the local magnitude M_L considering the attenuation function calibrated by Di Bona (2016). $\log A_0$ is computed considering $n = 1.667$, $k = 0.001736$ and the reference distance $D = 100$ km. M_L was computed for both the catalogs ($H71$ and NLL) and the histograms are shown in Fig. 14a.

The recorded magnitudes are distributed within a range of -1 to 4, with a peak between -0.5 and 2 (Fig. 14a) and no appreciable difference between the 2 catalogs can be observed. The completeness magnitude M_c of the H71 catalog, which represents the lowest magnitude in which all seismic events can reliably be recorded, was computed by using the EMR method (Entire Magnitude Range) proposed by (Woessner and Wiemer, 2005). This method, based on the consideration of the Gutenberg-Richter law (Gutenberg and Richter, 1956), enables the estimation of M_c by considering the entire range of event's magnitude, modeling both the complete and the incomplete part of the distribution. For our dataset $M_c = 0.82$ with a standard deviation $\sigma_{M_c} = 0.21$ (14b). This is a further confirmation of the CASP detection capability in identifying low-magnitude events. From a comparison between the range of magnitude calculated in this paper and the previous catalog (Filippucci et al., 2021) it

https://doi.org/10.5194/essd-2025-335
Preprint. Discussion started: 11 July 2025
© Author(s) 2025. CC BY 4.0 License.

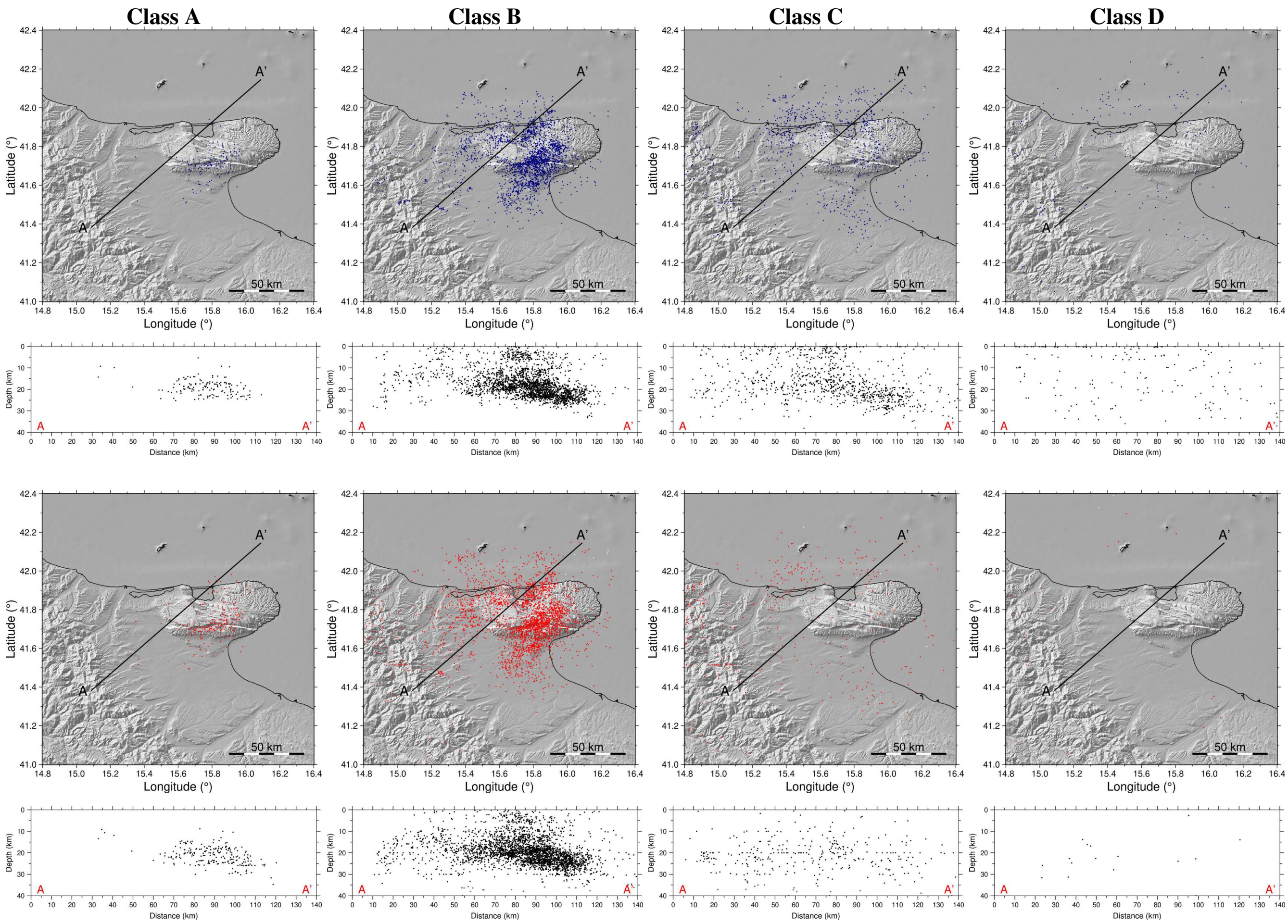

Figure 13. Maps of seismicity in quality classes as defined in Tab. 4. Black line on the map is a diameter of the investigation area oriented $45°$N corresponds to the vertical sections, plotted below each map for NLL (blue) and H71 (red), where all earthquakes are projected.

can be observed that the threshold of the minimum detectable magnitude is lowered to $M_L = -0.99$ respect to $M_LV = -0.1$, thus indicating an enhanced capability of earthquake detection. Regarding M_c, the comparison with the preceding catalog cannot be done due to the formulation used to compute the magnitude, the M_LV (the documentation can be found here: https://www.seiscomp.de/seiscomp3/doc/seattle/2014.084/apps/global_mlv.html, accessed on 30^{th} May 2025), which slightly underestimates the horizontal magnitude.

6 Discussion

The aim of our catalog is to detect the microseismicity of the GP so our interest is releated to low magnitude earthquakes. The OT network was designed to this purpose, in terms of network layout and type of instruments (Tallarico et al., 2025,

https://doi.org/10.5194/essd-2025-335
Preprint. Discussion started: 11 July 2025
© Author(s) 2025. CC BY 4.0 License.

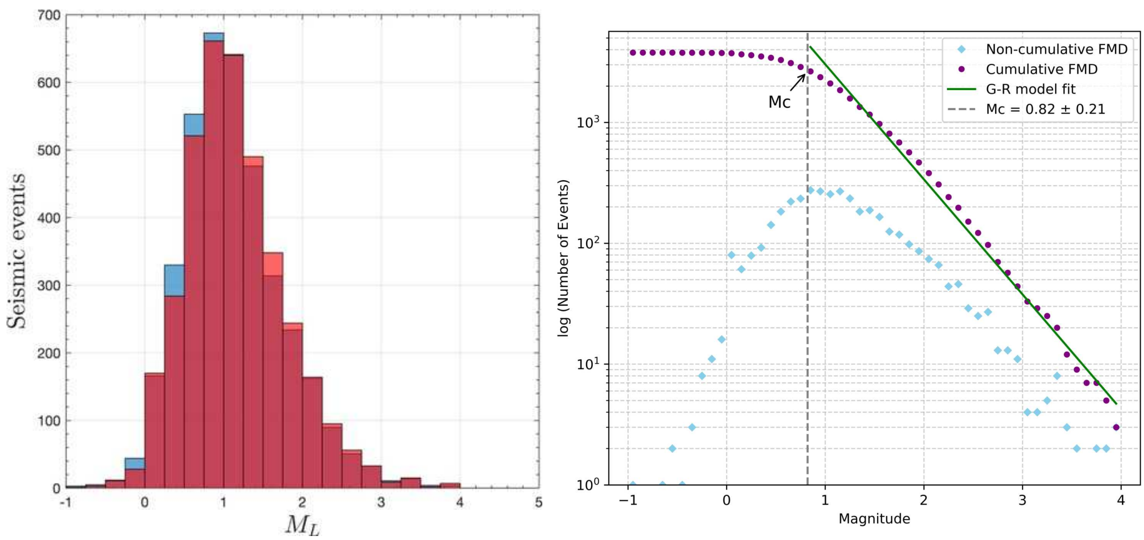

(a) (b)

Figure 14. a) Histogram of local magnitude M_L for the H71-catalog (orange), NLL-catalog (blue) and the overlapping areas (red). b) Frequency magnitude distribution (FMD) for the H71 catalog. Green line is the fit of the Gutenberg-Richter law between the computed M_C and the maximum magnitude value of the catalog. Blue diamonds and purple circles are, respectively, the non-cumulative and cumulative frequency magnitude distribution.

and reference therein). The dataset presented in this study collects the locations of earthquakes that occurred in the Gargano Promontory, a particularly characteristic area of the southern Apennines whose significant seismic hazard has not yet been explored in depth. Despite the geological and seismic importance of the region, studies on this area are limited, making further scientific investigation essential. The dataset developed in this study makes it possible to significantly improve knowledge of local seismicity, providing an indispensable basis for numerous geophysical studies, including seismo-tectonics studies, implementation of seismic velocity and attenuation models, tomography studies or site effects assessment. The choice of CASP allowed us to improve the seismic catalog by greatly increasing the number of collected earthquakes but some issues related to false location and non-tectonic events suggest that manual revision is a time-consuming operation but is still necessary to ensure reliability of the dataset of P and S phase arrivals and the consequent accuracy of earthquake locations. This discrimination is critical for an accurate seismic analysis of the area because the presence of quarry blasts can affect the results if not properly recognized. Therefore, the manual review of the automatic seismic catalog produced by CASP has proven to be essential to improve the quality of seismic data. By visual inspection we were able to recognize false events (together with bad located) and the quarry blasts, evaluated as the 30% and the 11% of the automatic catalog respectively. This revision highlighted that the main issue with the CASP software is the discrimination whether an event is an earthquake. Once that the earthquake is selected, the automatic location is of very good quality. The use of NLL and H71 for our P and S arrival times database is not so important, except for a group of earthquakes that NLL locates at shallow depths, with such a vertical error that in the error bar the events could be above the Earth's surface. These earthquakes are 418 and have an average depth of 1.95 ± 6.88 km and an

https://doi.org/10.5194/essd-2025-335
Preprint. Discussion started: 11 July 2025
© Author(s) 2025. CC BY 4.0 License.

average quality $\overline{q_f} = 6.3$ in the NLL catalog. The same events located with H71 result at an average depth of 14.56 ± 4.03 km and have an average $\overline{q_f} = 0.57$. For this reason, the locations obtained with H71 code seem more reliable than those obtained with NLL code, at least for that group of 418 earthquake. For the remaining 3402 earthquakes, average differences below 2 km are observed between the two catalogs, both horizontal and vertical.

Looking at the national bulletin provided by INGV, we found 836 and 822 earthquakes for NLL and H71 respectively in common with ONT catalog. Data of the ONT catalog can be found at https://terremoti.ingv.it/ (accessed on 30^{th} May 2025). Differences in locations are of the order of 1 km both in horizontal and 1 km in vertical. Differences are due to the number of stations used for locations and the velocity model. Regarding the computed magnitudes, we observed some differences in magnitude with the ONT bulletin that can be ascribed to the used attenuation law (Di Bona (2016) for our catalog and Hutton and Boore (1987) for the ONT), to the different locations, network geometry, type of instruments, number of recording stations. The greater number of earthquakes in our catalogs allowed to lower the magnitude threshold to values close to -1 (Fig. **??**) and thus providing a more detailed view of the microseismicity of the GP.

In Fig. 13 the location of the total earthquakes falling in classes A, B, C and D is shown. It is worth to note that the pattern of the seismicity plotted in the vertical section indicates the presence of a seismogenic layer between 15 and 25 km of depth. At this depth the major frequency in the histogram of the depths (Fig. 11) can be also observed. This seismogenic layer was already observed by Miccolis et al. (2021). The authors, with a dataset of 635 earthquakes found that GP seismicity is concentrated in the lower crust, aligned on a seismic layer that becomes deeper moving in NE direction towards the Adriatic Sea. Furthermore, the authors observed that most of the GP seismicity occurs in the area at north of the Mattinata fault (MF in Fig. 1b) with focal mechanisms mainly of transpressive type oriented in a NW-SE direction. In this paper we can confirm the existence of the same seismogenic layer in the lower crust with a dataset ten times larger than the previous one by Miccolis et al. (2021). It can also be observed that earthquakes seem clustered along the Mattinata fault, as was also visible in Miccolis et al. (2021), and a distribution of seismicity is observed along 2 alignments in SW-NE direction. In Fig. 13Class B, it is visible to the SE of the AA' profile, a denser cluster that seems to follow the shape of the seismogenic layer that deepens towards the NE, and the other with more scattered seismicity that is found over the AA' profile. Looking at the foci depth, it can be observed that:

- the shallower seismicity with hypocenters confined down to ≈ 10 km (yellow circles in Fig. A1d) is scarce and widespread all over the investigation area;
- deeper seismic activity can be found along a seismogenic layer in the lower crust down to ≈ 25 km (green circles in Fig. A1d) that was interpreted as due to fluid circulation from the mantle by Lavecchia et al. (2022);
- the intermediate seismicity (orange circles in Fig. A1d) is clustered along the Mattinata Fault (MF) toward S direction, confined at ≈ 15 km.

It is worth to note the absence of seismicity in the NE of GP. This peculiarity has been already observed and justified by the presence of a ductile upper crust in the thermo-rheological model of GP (Lavecchia et al., 2022). The presence of the seismic gap in NE of GP doesn't seem to depend on the network geometry. In fact in Fig. A1b,A1c,A1d we show the maps of epicenters

https://doi.org/10.5194/essd-2025-335
Preprint. Discussion started: 11 July 2025
© Author(s) 2025. CC BY 4.0 License.

recorded with three different network configuration adopted since 2013. Adding the stations OT13 and OT14 in NE of GP did not resolve this seismic gap but increased the number of recorded earthquakes NE offshore. Another seismic gap is present in the area between stations APRC and SGRT (Fig. A1a) that cannot be ascribed to the network density. The OT network geometry evolution does not affect detection rate in the period 2013-2022 (blue line in Fig. A2). The detection rate of the ONT catalog is positively affected by the acquisition of the OT network by EIDA-INGV, as witnessed by the sharp change in the slope of the cumulative number of detected events in GP (dashed line in Fig. A2). The flat trend in the cumulative curve of CASP (this work) (Fig A2) belongs to the period between 2018 and 2019 and corresponds to the updates of the network data transmission systems required for data sharing on EIDA (as described by Filippucci et al., 2021).

7 Data Availability

The NLL catalog and H71 catalog are available on Mendeley Data (Ferreri et al., 2025) at https://doi.org/10.17632/nhfvx7ysxw.3. These datasets were collected by using the recordings of the GSN network (as described in Section 2) composed by stations of the OT network (University of Bari "Aldo Moro", 2013) and by stations of IV network (Istituto Nazionale di Geofisica e Vulcanologia (INGV), 2005).

8 Conclusions

In this work we have built a new dataset of earthquakes in the GP area in southern Italy, collected using the CASP software detect and the OTRIONS network recordings in the decade from 2013 to 2022. Manual review work was necessary and indispensable to discriminate the type of automatic event provided by the software and eliminate both false and poorly localized earthquakes and quarry blasts. The use of CASP represented an important step to collect a robust dataset of earthquakes. However, to improve the potential of this software, in the future it will be necessary to continue to improve the automatic detection and picking algorithms, to reduce the time costs of manual review by the operator. The results are released in two catalogs of about 3800 earthquakes localized with 2 different methods, non-linear and linearized (NLL and H71 respectively). We observed differences in 418 locations probably due to the difficulty of NLL to adapt the localization grid to the network geometry. The quality of the localizations was calculated with a formula inspired by that proposed for the Italian earthquake catalog (Michele et al., 2019), adapted for the GP area and applied to the 2 catalogs with different normalization factors. In general, the location quality, despite the large azimuthal gap of the GP preventing optimal locations, is of good/medium quality and confirms the presence of a seismogenic layer in the lower crust, observed in previous studies (Miccolis et al., 2021), site of intense low-magnitude seismic activity and shows an intense seismogenic activity along the MF at intermediate depths. Shallow seismicity seems scarce and scattered all over the investigation area. As regard the network coverage of the GP, the area over the coast line and offshore in the N of GP has been recently affected by an intense seismic activity with the major earthquake of $M_L = 4.7$ occurred 14th March 2025 (https://terremoti.ingv.it/, accessed 04/06/2025), the most energetic event ever instrumentally recorded in this area. This seismic sequence highlights the crucial role of the OT network in the seismic

https://doi.org/10.5194/essd-2025-335
Preprint. Discussion started: 11 July 2025
© Author(s) 2025. CC BY 4.0 License.

monitoring of the area, a task carried out by INGV with surveillance purposes on behalf of the Italian Department of Civil Protection.

Appendix A: Supplementary material

A1 Network performance

In Table A1 the performance of the GSN stations during the period 2013-2022. Regarding the OT stations, an evident increase can be observed in the ratio between working days/expected working days in the years after 2019, thanks to the change in the data acquisition system of OT network. Regarding the IV stations, any particular variations are observed in the considered decade. Empty cells indicate not working periods.

The network performance and the network geometry can affect the geometry of the distribution of the recorded earthquakes. In Fig. A1 the plot of the seismicity related to 3 different periods (Fig. A1a, A1b, A1c) of the network operation is shown together with the entire period (Fig. A1d).

https://doi.org/10.5194/essd-2025-335
Preprint. Discussion started: 11 July 2025
© Author(s) 2025. CC BY 4.0 License.

		Working days/Expected working days Year									
Network	**Station**	**2013**	**2014**	**2015**	**2016**	**2017**	**2018**	**2019**	**2020**	**2021**	**2022**
OT	OT01	95%									
OT	OT02	100%	100%								
OT	OT03	100%	98%	89%	77%	82%	54%	54%	89%	100%	97%
OT	OT04	94%	71%	93%	86%	87%	65%	55%	98%	100%	95%
OT	OT05	60%	0%	35%	76%	68%	65%	47%	92%	100%	95%
OT	OT06	81%	44%	34%	84%	84%	61%	52%	99%	100%	96%
OT	OT07	76%	78%	76%	85%	88%	63%	30%	13%	100%	97%
OT	OT08	41%	29%	39%							
OT	OT09	89%	73%	9%							
OT	OT10	83%	30%	31%	70%	57%	61%				
OT	OT11	67%	18%	71%	87%	85%	45%	32%	83%	93%	97%
OT	OT12	78%	5%	58%	63%	76%	24%	66%	51%	93%	97%
OT	OT13			97%	78%	76%	61%	49%	92%	100%	97%
OT	OT14			74%	74%	78%	49%	54%	18%	100%	97%
OT	OT16									100%	91%
OT	OT17									98%	97%
IV	APRC				93%	99%	99%	99%	90%	93%	91%
IV	CAPA		84%	96%	88%	75%	81%	55%	90%	67%	11%
IV	CIGN	98%	94%	84%	96%	100%	97%	100%	94%	61%	1%
IV	GATE	99%	100%	100%	100%	100%	100%	100%	95%	66%	91%
IV	MELA	98%	100%	99%	92%	100%	99%	99%	100%	95%	91%
IV	MOCO	97%	99%	99%	99%	97%	99%	94%	91%	96%	99%
IV	MSAG	99%	100%	100%	83%	55%	99%	99%	98%	100%	100%
IV	SGRT	99%	100%	100%	100%	100%	86%	86%	81%	100%	76%
IV	SGTA	98%	100%	88%	97%	96%	100%	99%	100%	93%	100%
IV	TREM		54%	87%	99%	76%	47%	0%	48%	98%	100%

Table A1. Performance of GSN in the period 2013-2022.

https://doi.org/10.5194/essd-2025-335
Preprint. Discussion started: 11 July 2025
© Author(s) 2025. CC BY 4.0 License.

Open Access Earth System Science Data Discussions

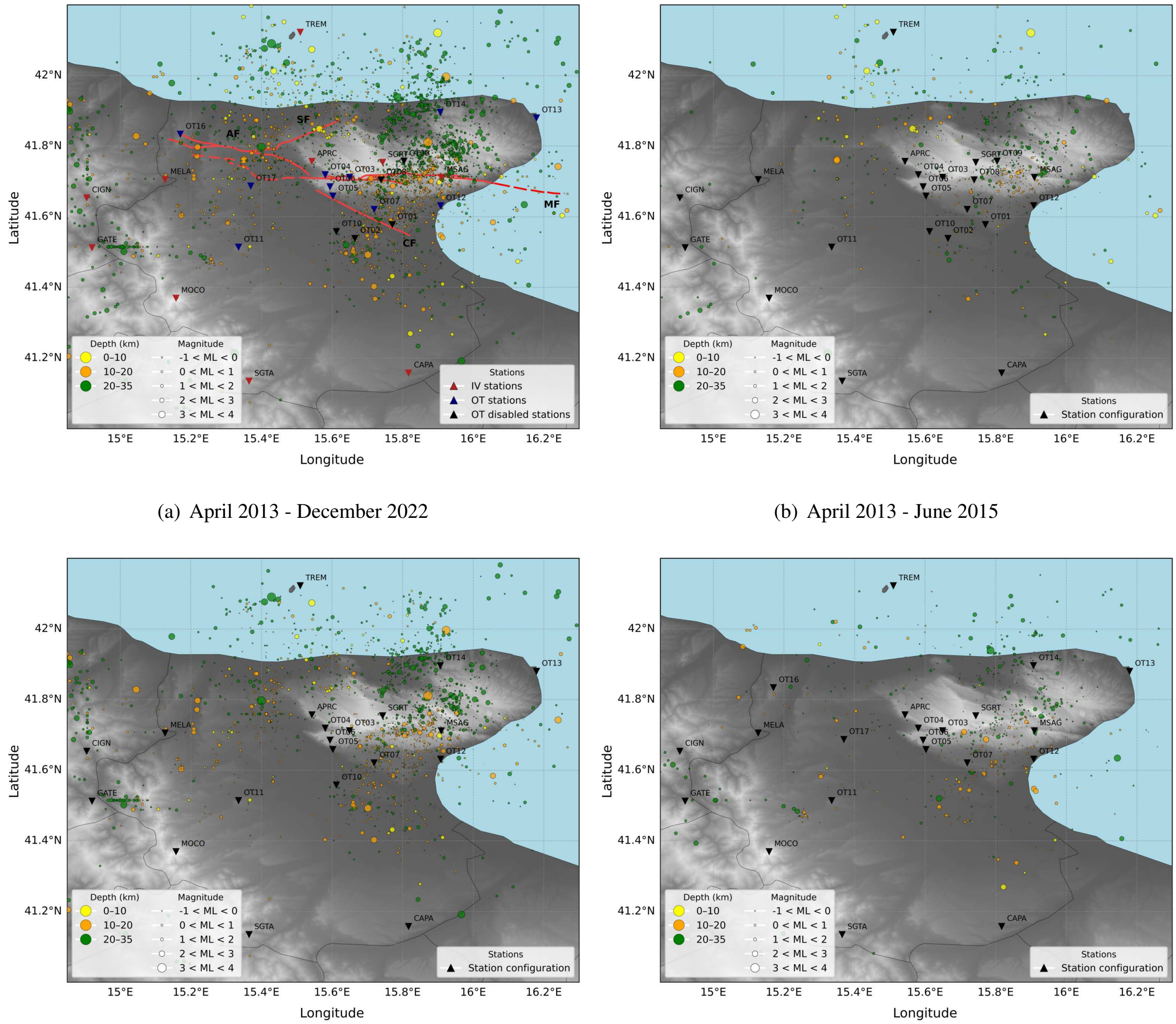

(a) April 2013 - December 2022

(b) April 2013 - June 2015

(c) July 2015 - March 2021

(d) April 2021 - December 2022

Figure A1. Maps of the epicenters of the H71 catalog with time. Circle dimension is proportional to M_L, color refers to depth, as indicated in the superimposed legend. a) Plot of the seismicity for the entire period, from April 2013 to December 2022; colored triangles refer to network (red for IV, blue for OT, black for OT disabled, as indicated in the superimposed legend). b) From April 2013 to June 2015; c) from July 2015 to March 2021; d) from April 2021 to December 2022; black triangles indicate the GSN stations.

The cumulative number of earthquakes detected in this work by using CASP software and detected by Italian ONT are plotted in Fig. A2.

https://doi.org/10.5194/essd-2025-335
Preprint. Discussion started: 11 July 2025
© Author(s) 2025. CC BY 4.0 License.

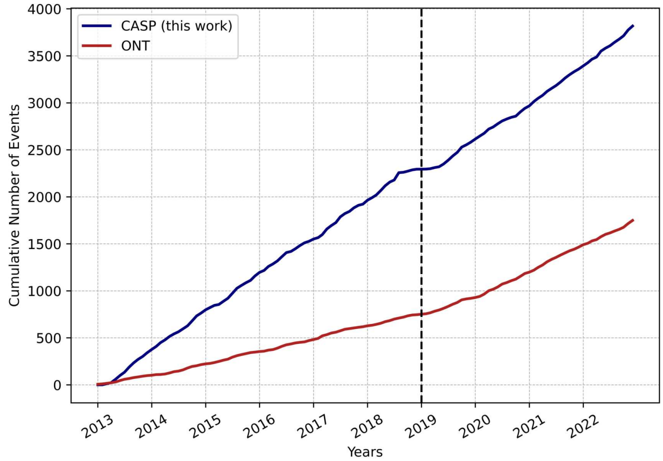

Figure A2. Detection rate as cumulative number of detected events per month for the ONT catalog (red line) and for this work (blue line). The dashed line indicates the acquisition of OT stations by ONT.

A2 PPSDs

In this section, we exhibit the Probability Power Spectral Densities (PPSDs) calculated for the OT seismic stations of the GSN. See the main text for details. Fig. A3 shows the PPSDs of stations OT01, OT02, OT03, OT04, the Fig. A4 shows stations OT05, OT06, OT07, OT08, the Fig. A5 shows stations OT09, OT10, OT11, OT12, and the Fig. A6 the stations OT13, OT14, OT16, OT17.

https://doi.org/10.5194/essd-2025-335
Preprint. Discussion started: 11 July 2025
© Author(s) 2025. CC BY 4.0 License.
Open Access Earth System Science Data Discussions

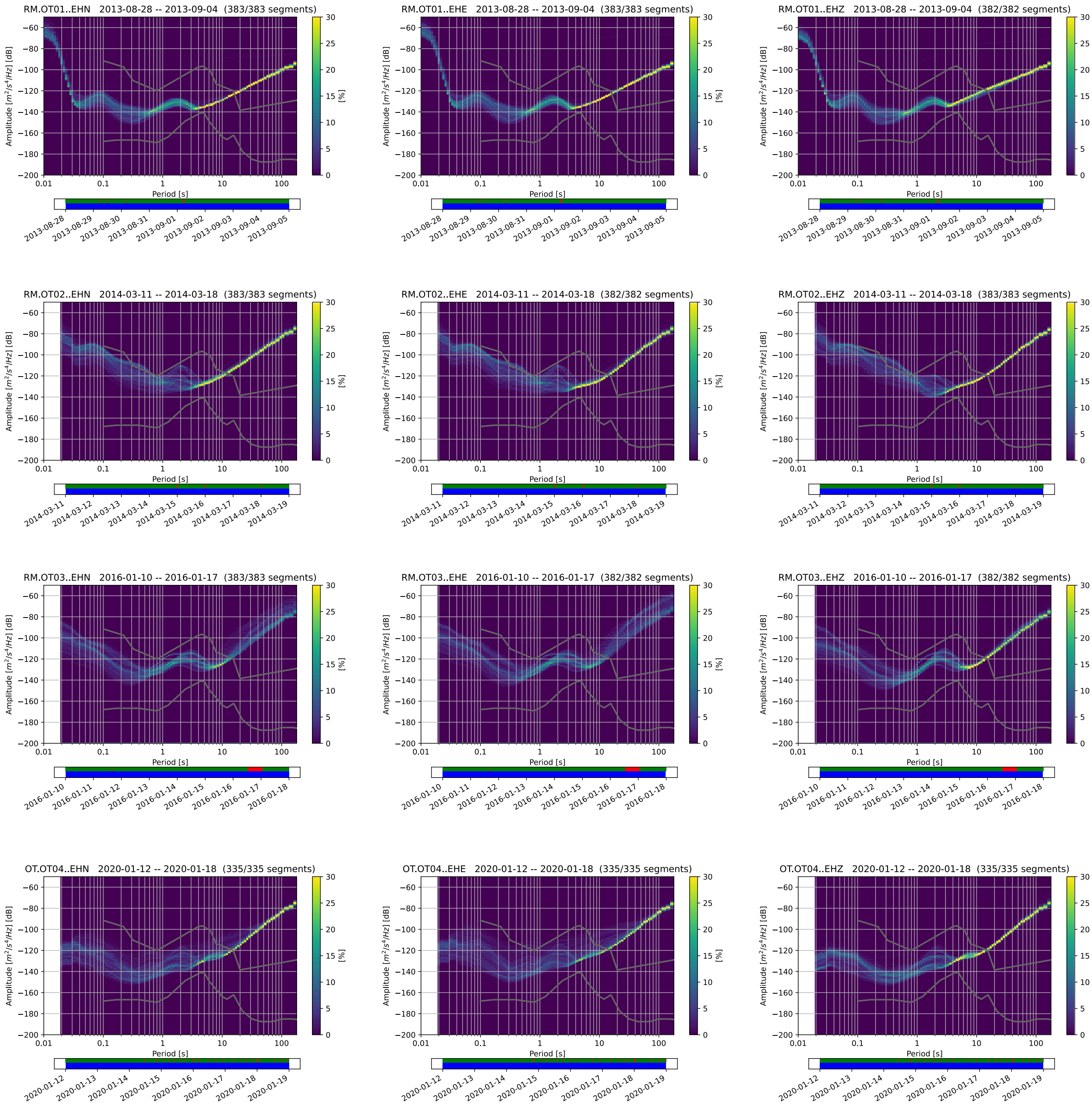

Figure A3. PPSDs of the three components of OT01, OT02, OT03, OT04.

https://doi.org/10.5194/essd-2025-335
Preprint. Discussion started: 11 July 2025
© Author(s) 2025. CC BY 4.0 License.

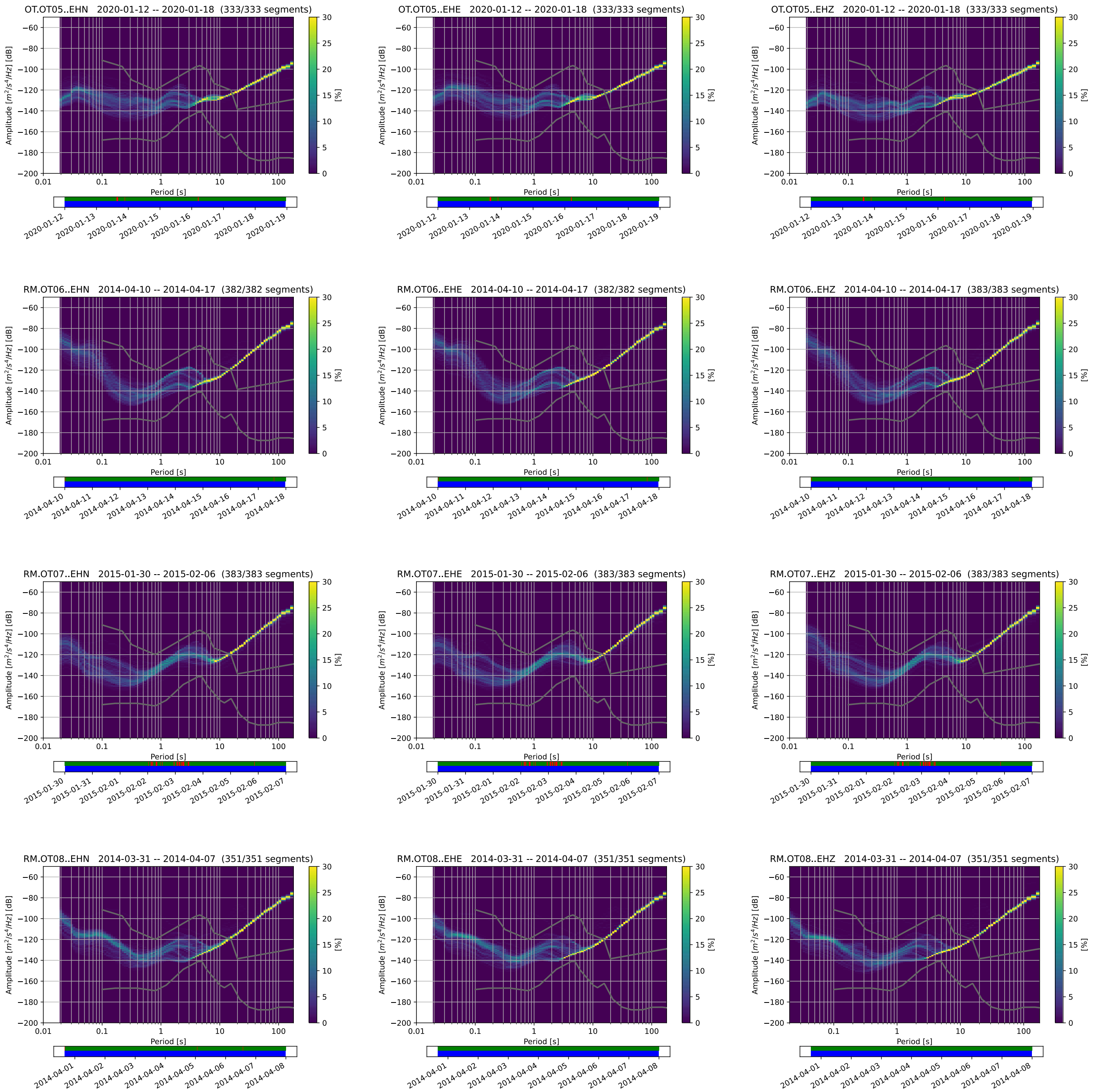

Figure A4. PPSDs of the three components of OT05, OT06, OT07, OT08.

https://doi.org/10.5194/essd-2025-335
Preprint. Discussion started: 11 July 2025
© Author(s) 2025. CC BY 4.0 License.

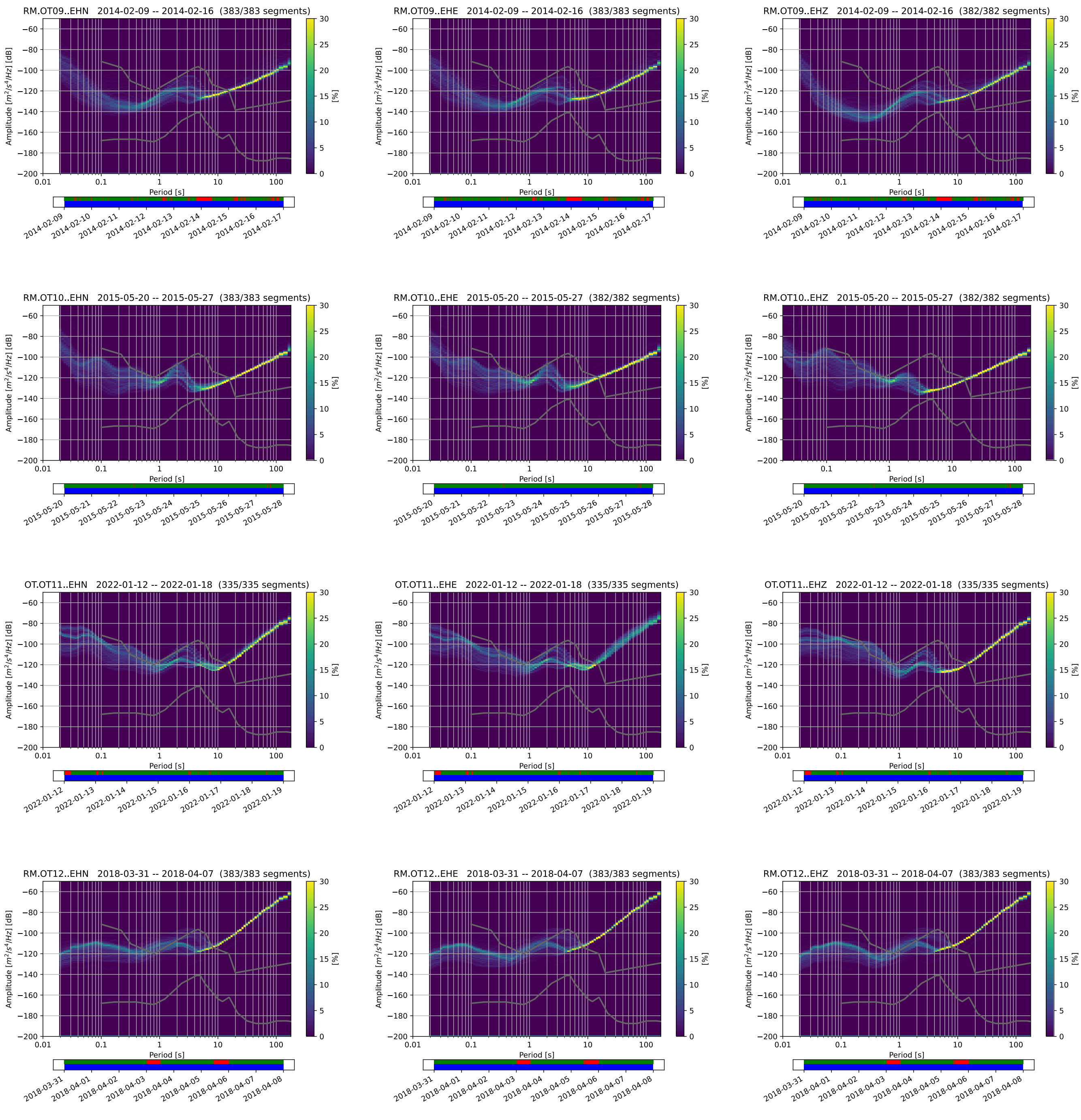

Figure A5. PPSDs of the three components of OT09, OT10, OT11, OT12.

https://doi.org/10.5194/essd-2025-335
Preprint. Discussion started: 11 July 2025
© Author(s) 2025. CC BY 4.0 License.

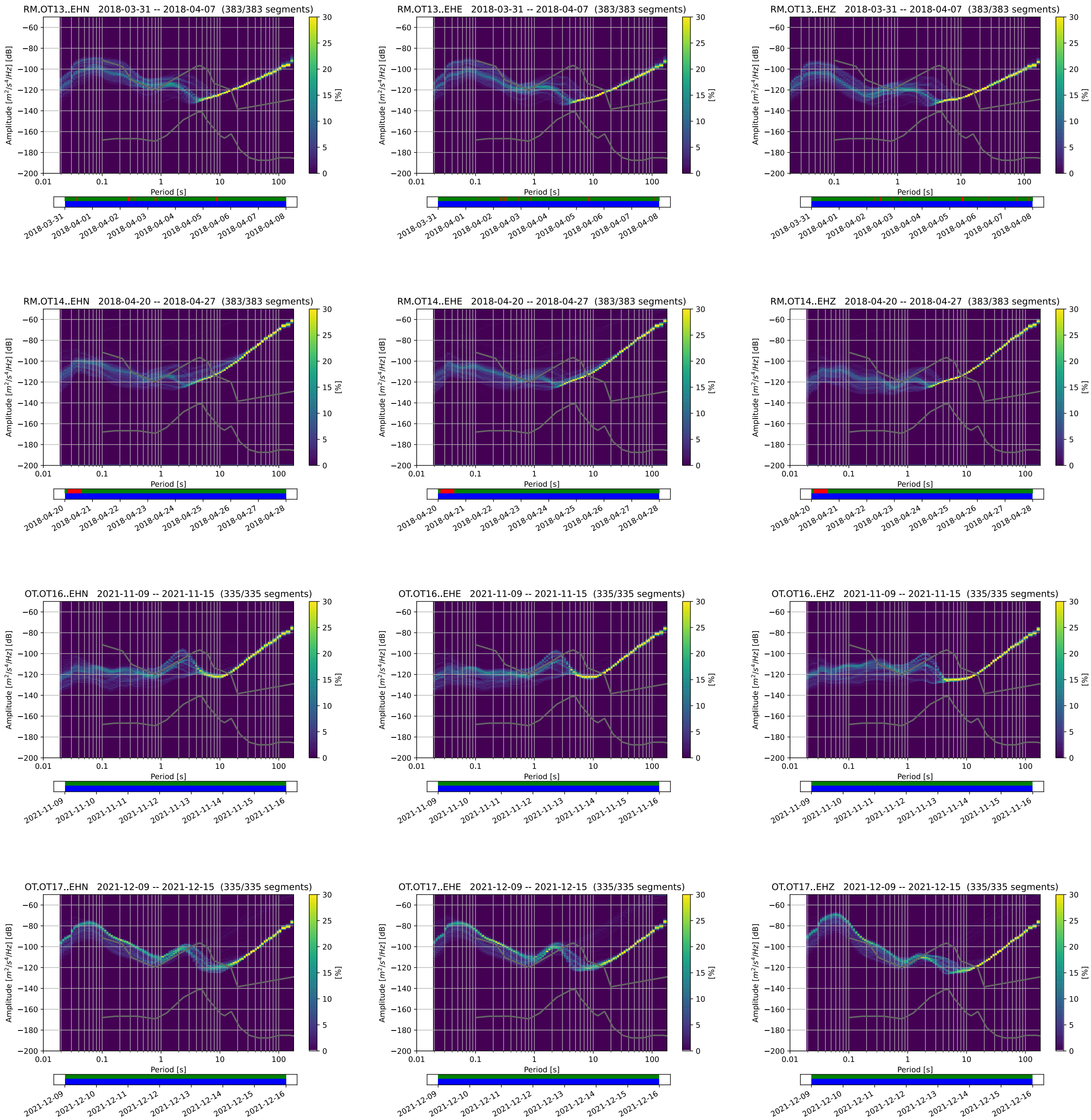

Figure A6. PPSDs of the three components of OT13, OT14, OT16, OT17.

https://doi.org/10.5194/essd-2025-335
Preprint. Discussion started: 11 July 2025
© Author(s) 2025. CC BY 4.0 License.

A3 Graphical Abstract

The following figure (Fig. A7) summarizes the results.

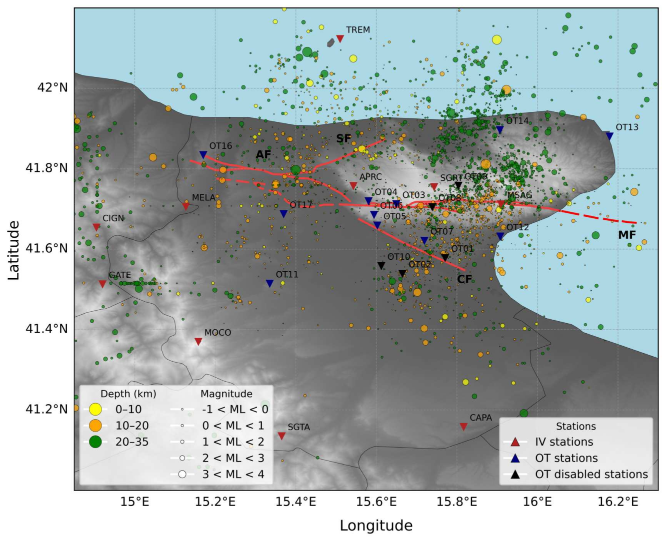

Figure A7. Maps of the epicenters of the H71 catalog with time. Circle dimension is proportional to M_L, color refers to depth, as indicated in the superimposed legend. Plot of the seismicity for the entire period, from April 2013 to December 2022

Code availability. The code CASP is available under license at https://lunitek.it/seismic/seismic-software/casp/ (last accessed on 30th May 2025); NLL and H71 codes are available for free; MATLAB (MathWorks ®) code was used for histograms and for the map in Figure 7 and is available under license; Maps and codes were written with python language, available for free. The manuscript was written with Overleaf, available for free.

Data availability. The NLL catalog and H71 catalog are available on Mendeley Data (Ferreri et al., 2025) at https://doi.org/10.17632/nhfvx7ysxw.3 (accessed on 09th June 2025)

Author contributions. Conceptualization APF, MF, GS, AT; Data curation AR, GC, LF; Formal analysis APF, AR, RG, TN, MM, Funding acquisition GS, AT; Methodology APF, MF, TN, AT; Visualization APF, AR, RG, TN, AT; all the authors participated to the validation and to the writing of the paper.

Competing interests. No competing interests are present.

© Author(s) 2025. CC BY 4.0 License.

Acknowledgements. We wish to thank Anthony Lomax for his help in project and writing the input file per NLL (Lomax et al., 2000) software for earthquake location.

RETURN Project (Multi-Risk science for resilient commUnities undeR a changiNg climate) Extended Partnership in the framework of European Union—NextGenerationEU (National Recovery and Resilience Plan—NRRP, Mission 4, Component 2, Investment 1.3—D.D. 1243 2/8/2022, PE0000005).

MEET Project (Monitoring Earth's Evolution and Tectonics) in the framework of National Recovery and Resilience Plan (PNRR) - Mission 4, "Education and Research" - Component 2, "From research to business" - Investment line 3.1, "Fund for the creation of an integrated system of research and innovation. infrastructures" - project code IR0000025.

We declare that any part of this work was generated with AI tools.

https://doi.org/10.5194/essd-2025-335
Preprint. Discussion started: 11 July 2025
© Author(s) 2025. CC BY 4.0 License.

References

Abbasi, A.: Linear and nonlinear earthquake location approaches in a case study overview, Physics of the Earth and Planetary Interiors, 293, 106 265, 2019.

Chilovi, C., de Feyter, A. J., and Pompucci, A.: Wrench zone reactivation in the Adriatic Block; the example of the Mattinata fault system (SE Italy), Italian Journal of Geosciences, 119, 3–8, 2000.

De Gori, P., Lucente, F. P., Govoni, A., Margheriti, L., and Chiarabba, C.: Seismic swarms in the Pollino seismic gap: Positive fault inversion within a popup structure, Frontiers in Earth Science, 10, 968 187, 2022.

Del Gaudio, V., Pierri, P., Frepoli, A., Calcagnile, G., Venisti, N., and Cimini, G.: A critical revision of the seismicity of Northern Apulia (Adriatic microplate — Southern Italy) and implicationsfor the identification of seismogenic structures, Tectonophysics, 436, 9–35, https://doi.org/https://doi.org/10.1016/j.tecto.2007.02.013, 2007.

Di Bona, M.: A Local Magnitude Scale for Crustal Earthquakes in Italy, Bulletin of the Seismological Society of America, 106, 242–258, https://doi.org/10.1785/0120150155, 2016.

Doglioni, C., Mongelli, F., and Pieri, P.: The Puglia uplift (SE Italy): An anomaly in the foreland of the Apenninic subduction due to buckling of a thick continental lithosphere, Tectonics, 13, 1309–1321, https://doi.org/10.1029/94TC01501, 1994.

Ebel, J. E.: The importance of small earthquakes, Seismological Research Letters, 79, 491–493, 2008.

Ferreri, A. P., Romeo, A., Giannuzzi, R., Cecere, G., Falco, L., Filippucci, M., Michele, M., Ninivaggi, T., Selvaggi, G., and Tallarico, A.: The new seismic catalog of the Gargano area (Southern Italy) after a decade of seismic monitoring by OTRIONS network, https://doi.org/10.17632/nhfvx7ysxw.3, 2025.

Festa, V., Tripaldi, S., Siniscalchi, A., Acquafredda, P., Fiore, A., Mele, D., and Romano, G.: Geoelectrical resistivity variations and lithological composition in coastal gypsum rocks: A case study from the Lesina Marina area (Apulia, southern Italy), Engineering Geology, 202, 163–175, https://doi.org/https://doi.org/10.1016/j.enggeo.2015.12.026, 2016.

Filippucci, M., Del Pezzo, E., de Lorenzo, S., and Tallarico, A.: 2D kernel-based imaging of coda-Q space variations in the Gargano Promontory (Southern Italy), Physics of the Earth and Planetary Interiors, 297, 106 313, 2019a.

Filippucci, M., Tallarico, A., Dragoni, M., and De Lorenzo, S.: Relationship between depth of seismicity and heat flow: the case of the Gargano area (Italy), Pure and Applied Geophysics, 176, 2383–2394, 2019b.

Filippucci, M., Miccolis, S., Castagnozzi, A., Cecere, G., de Lorenzo, S., Donvito, G., Falco, L., Michele, M., Nicotri, S., Romeo, A., Selvaggi, G., and Tallarico, A.: Seismicity of the Gargano promontory (Southern Italy) after 7 years of local seismic network operation: Data release of waveforms from 2013 to 2018, Data in Brief, 35, 106 783, https://doi.org/https://doi.org/10.1016/j.dib.2021.106783, 2021.

Govoni, A., Margheriti, L., Moretti, M., Chiarabba, C., D'Alema, E., Marzorati, S., Franceschi, D., De Gori, P., Carluccio, I., Delladio, A., Cecere, G., D'Ambrosio, C., Danecek, P., Della Bina, E., Fares, M., Lucente, F. P., Braun, T., Pintore, S., and Gervasi, A.: Seismic Data acquired by the INGV Emergency Group - Pollino-Italy 2011 - T07, https://doi.org/10.13127/SD/SX4PYRLDWA, 2023.

Gulia, L.: Detection of quarry and mine blast contamination in European regional catalogues, Natural Hazards, 53, 229–249, https://doi.org/10.1007/s11069-009-9426-8, 2010.

Gulia, L. and Gasperini, P.: Contamination of Frequency–Magnitude Slope (b–Value) by Quarry Blasts: An Example for Italy, Seismological Research Letters, 92, https://doi.org/10.1785/0220210080, 2021.

Gutenberg, B. and Richter, C. F.: Earthquake magnitude, intensity, energy, and acceleration, Bulletin of the seismological society of America, https://doi.org/10.1785/BSSA0320030163, 1956.

https://doi.org/10.5194/essd-2025-335
Preprint. Discussion started: 11 July 2025
© Author(s) 2025. CC BY 4.0 License.

Hutton, L. and Boore, D. M.: The ML scale in southern California, Bulletin of the Seismological Society of America, 77, 2074–2094, 1987.

Iannaccone, G., Zollo, A., Elia, L., Convertito, V., Satriano, C., Martino, C., Festa, G., Lancieri, M., Bobbio, A., Stabile, T., et al.: A prototype system for earthquake early-warning and alert management in southern Italy, Bulletin of Earthquake Engineering, 8, 1105–1129, 2010.

Istituto Nazionale di Geofisica e Vulcanologia (INGV): Rete Sismica Nazionale (RSN), https://doi.org/10.13127/SD/X0FXNH7QFY, 2005.

Lavecchia, A., Filippucci, M., Tallarico, A., Selvaggi, G., Cecere, G., and Cloetingh, S.: Role of crustal fluids and thermo-mechanical structure for lower crustal seismicity: The Gargano Promontory (southern Italy), Global and Planetary Change, 217, 103 929, 2022.

Lee, W. H. and Lahr, J. C.: HYPO71 (revised; a computer program for determining hypocenter, magnitude, and first motion pattern of local earthquakes, Tech. rep., US Dept. of the Interior, Geological Survey, National Center for Earthquake . . . , 1975.

Li, Z.: Recent advances in earthquake monitoring I: Ongoing revolution of seismic instrumentation, Earthquake science, 34, 177–188, 2021.

Lomax, A., Virieux, J., Volant, P., and Berge-Thierry, C.: Probabilistic Earthquake Location in 3D and Layered Models, pp. 101–134, Springer Netherlands, Dordrecht, ISBN 978-94-015-9536-0, https://doi.org/10.1007/978-94-015-9536-0_5, 2000.

Lomax, A., Michelini, A., and Curtis, A.: EarthquakeEarthquakeLocationEarthquakelocation, Direct, Global-SearchGlobal-searchMethods, pp. 2449–2473, Springer New York, New York, NY, ISBN 978-0-387-30440-3, https://doi.org/10.1007/978-0-387-30440-3_150, 2009.

Lucente, S., Ninivaggi, T., de Lorenzo, S., Del Pezzo, E., Filippucci, M., Prosser, G., and Tallarico, A.: Q β, Q c, Q i, Q s of the Gargano Promontory (Southern Italy), Journal of Seismology, 27, 827–846, 2023.

McNamara, D. E. and Buland, R. P.: Ambient Noise Levels in the Continental United States, Bulletin of the Seismological Society of America, 94, 1517–1527, https://doi.org/10.1785/012003001, 2004.

Miccolis, S., Filippucci, M., Lorenzo, S., Frepoli, A., Pierri, P., and Tallarico, A.: Seismogenic Structure Orientation and Stress Field of the Gargano Promontory (Southern Italy) From Microseismicity Analysis, Frontiers in Earth Science, 09, 589 332, https://doi.org/10.3389/feart.2021.589332, 2021.

Michele, M., Latorre, D., and Emolo, A.: An Empirical Formula to Classify the Quality of Earthquake Locations, Bulletin of the Seismological Society of America, 109, 2755–2761, https://doi.org/10.1785/0120190144, 2019.

Mongelli, F. and Ricchetti, G.: Heat flow along the candelaro fault — gargano headland (Italy), Geothermics, 2, 450–458, https://doi.org/10.1016/0375-6505(70)90043-X, 1970.

Passarelli, L., Roessler, D., Aladino, G., Maccaferri, F., Moretti, M., Lucente, F. P., Braun, T., De Gori, P., Margheriti, L., Woith, H., Sebastian, H., Eleonora, R., and Dahm, T.: Pollino Seismic Experiment (2012-2014), https://doi.org/10.14470/9N904956, 2012.

Passarelli, L., Govoni, A., Maccaferri, F., Woith, H., Strollo, A., Zieke, T., Margheriti, L., Martinelli, G., and Dahm, T.: East Pollino Experiment, Southern Italy, https://doi.org/10.14470/LM582526, 2017.

Patacca, E. and Scandone, P.: The 1627 Gargano earthquake (Southern Italy): Identification and characterization of the causative fault, Journal of Seismology, 8, 259–273, https://doi.org/10.1023/B:JOSE.0000021393.77543.1e, 2004.

Peterson, J. R.: Observations and modeling of seismic background noise, Tech. rep., US Geological Survey, 1993.

Pierri, P., Filippucci, M., Del Gaudio, V., Tallarico, A., Venisti, N., and Festa, V.: Ostuni..., Applied Science, 2024.

Presti, D., Orecchio, B., Falcone, G., and Neri, G.: Linear versus non-linear earthquake location and seismogenic fault detection in the southern Tyrrhenian Sea, Italy, Geophysical Journal International, 172, 607–618, 2008.

Rovida, A., Locati, M., Romano, C., Lolli, B., and Gasperini, P.: Catalogo Parametrico dei Terremoti Italiani, versione CPTI15, https://doi.org/10.6092/INGV.IT-CPTI15, 2016.

https://doi.org/10.5194/essd-2025-335
Preprint. Discussion started: 11 July 2025
© Author(s) 2025. CC BY 4.0 License.

Salvi, S., Quattrocchi, F., Brunori, C. A., Doumaz, F., Angelone, M., Billi, A., Buongiorno, M. F., Funiciello, R., Guerra, M., Mele, G., Pizzino, L., and Salvini, F.: A Multidisciplinary Approach to Earthquake Research: Implementation of a Geochemical Geographic Information System for the Gargano Site, Southern Italy, Natural Hazards, 20, 255–278, https://doi.org/10.1023/A:1008105621134, 1999.

Scafidi, D., Viganò, A., Ferretti, G., and Spallarossa, D.: Robust Picking and Accurate Location with RSNI-Picker2: Real-Time Automatic Monitoring of Earthquakes and Nontectonic Events, Seismological Research Letters, 89, 1478–1487, https://doi.org/10.1785/0220170206, 2018.

Scafidi, D., Spallarossa, D., Ferretti, G., Barani, S., Castello, B., and Margheriti, L.: A Complete Automatic Procedure to Compile Reliable Seismic Catalogs and Travel-Time and Strong-Motion Parameters Datasets, Seismological Research Letters, 90, 1308–1317, https://doi.org/10.1785/0220180257, 2019.

Spallarossa, D., Bindi, D., Augliera, P., and Cattaneo, M.: An ML scale in northwestern Italy, Bulletin of the Seismological Society of America, 92, 2205–2216, 2002.

Spallarossa, D., Cattaneo, M., Scafidi, D., Michele, M., Chiaraluce, L., Segou, M., and Main, I.: An automatically generated high-resolution earthquake catalogue for the 2016–2017 Central Italy seismic sequence, including P and S phase arrival times, Geophysical Journal International, 225, 555–571, 2021.

Stabile, T. A., Serlenga, V., Satriano, C., Romanelli, M., Gueguen, E., Gallipoli, M. R., Ripepi, E., Saurel, J.-M., Panebianco, S., Bellanova, J., and Priolo, E.: The INSIEME seismic network: a research infrastructure for studying induced seismicity in the High Agri Valley (southern Italy), Earth System Science Data, 12, 519–538, https://doi.org/10.5194/essd-12-519-2020, 2020.

Tallarico, A.: Rete multi-parametrica per lo studio e il monitoraggio dei rischi naturali nel canale d'Otranto e nel Mar Ionio, Ragusa Service, ISBN 9788890670763, 2015.

Tallarico, A., Patella, D., Ninivaggi, T., Ruzza, G., Cecere, G., Filippucci, M., and Selvaggi, G.: The OTRIONS seismic network: instrumentation upgrade and borehole installation, Annals of Geophysics, under review, https://doi.org/https://doi.org/10.4401/ag, 2025.

Tramelli, A., Orazi, M., Nardone, L., Bobbio, A., Benincasa, A., Buonocunto, C., Capello, M., Caputo, A., Castellano, M., D'Auria, L., Cesare, W. D., Filippo, A. D., Galluzzo, D., Gaudiosi, G., Giudicepietro, F., Liguoro, F., Bascio, D. L., Martini, M., Martino, C., Peluso, R., Ricciolino, P., Scarpato, G., Torello, V., and Bianco, F.: The seismic network of Ischia island from 1993 to 2021, Geological Society, London, Special Publications, 519, 47–58, https://doi.org/10.1144/SP519-2021-192, 2024.

University of Bari "Aldo Moro": OTRIONS, https://doi.org/10.7914/SN/OT, 2013.

Ventola, I., Balasco, M., De Girolamo, M., Falco, L., Filippucci, M., Hillmann, L., Romano, G., Serlenga, V., Stabile, T. A., Strollo, A., Tallarico, A., Tripaldi, S., Zieke, T., and Siniscalchi, A.: Seismic-electromagnetic signals from two monitoring stations in Southern Italy: Electromagnetic time series release, Geoscience Data Journal, n/a, https://doi.org/https://doi.org/10.1002/gdj3.262, 2024.

Woessner, J. and Wiemer, S.: Assessing the Quality of Earthquake Catalogues: Estimating the Magnitude of Completeness and Its Uncertainty, Bulletin of the Seismological Society of America, 95, 684–698, https://doi.org/10.1785/0120040007, 2005.